Chapter 17
FMRI Using Exogenous Agents and Cerebral Blood Volume Contrast

Joseph B. Mandeville

Abstract The most robust techniques for fMRI employ gradient-echo imaging to measure task-induced changes in MRI signal resulting from endogenous or exogenous paramagnetic contrast agents within the bloodstream. In animal models, blood magnetization can be adjusted to optimal levels using injected agent, and fMRI then reflects dynamic changes in cerebral blood volume (CBV). In the absence of injected agent, blood magnetization, and signal changes are smaller, and blood oxygen level dependent (BOLD) signal reports a more complex physiology that depends upon changes in blood volume, flow, and oxygen utilization. This chapter focuses primarily upon the physics and physiology of dynamic fMRI measurements of CBV using exogenous contrast agent, both as a useful tool for fMRI applications and as a method that contributes to our understanding of BOLD signal. Other recent techniques to measure CBV using endogenous mechanisms also are described briefly, as well as the fMRI method for assessing changes in cerebral blood flow by arterial spin labeling. Together, these techniques are expanding the portfolio of useful fMRI methods beyond BOLD signal and contributing to our understanding of the physiological mechanisms underlying the BOLD phenomenon.

Keywords Arterial spin labeling • ASL • BOLD • CBF • CBV • Cerebral blood flow • Cerebral blood volume • Cerebral metabolic rate of oxygen utilization • CMRO2 • CNR • Contrast to noise ratio • Delayed compliance • Feraheme • fMRI • Hemodynamic response function • Impulse response function • IRON • MION • MRI • Relaxation rate • Relaxation time • Signal to noise ratio • SNR • Undershoot • USPIO • VASO • VERVE

J.B. Mandeville, Ph.D. (✉)
Athinoula A. Martinos Center for Biomedical Imaging, Massachusetts General Hospital, Charlestown, MA 02155, USA
e-mail: jbm@nmr.mgh.harvard.edu

17.1   Introduction

As a tool for assessing brain function, magnetic resonance imaging (MRI) plays multiple roles by providing relatively direct information about metabolic substrates (spectroscopy), or by providing information about neuro-metabolic status that, while indirect, can be obtained with excellent spatial and temporal resolution that is highly desirable for many applications in neuroscience and investigations of pathophysiology. The functional MRI (fMRI) techniques that are most commonly employed today are based upon the assumption that regional brain activity is coupled to the blood supply, as postulated more than a century ago (Roy and Sherrington 1890). Through flow-metabolism coupling, fMRI is thought to represent a summation of competing metabolic processes; as such, changes in brain activity can be localized, but additional information generally is required to interpret findings in terms of the underlying neurotransmission and neurochemistry.

Prior to neuro-imaging, inferences about brain organization and function were derived from lesion and postmortem observations in humans and invasive studies in animal models. Most modern non-invasive imaging methods can be traced back to invasive imaging techniques developed in animal models in the 1970s and earlier. Arterial spin labeling (ASL) by MRI is analogous to the positron emission tomography (PET) method using radiolabeled water (Ter-Pogossian et al. 1969), a method that in turn adapted the radiolabeled diffusible tracers employed by autoradiography (Kety 1960). Bolus measurements of cerebral blood flow (CBF) and volume (CBV) using MRI contrast agents follow the same method employed by x-ray computed tomography using iodinated contrast agent (Axel 1980), which in turn is based upon indicator dilution theory and earlier methods of sampling contrast material (Meier and Zierler 1954). Much of the physics and physiology of the BOLD technique can be related to earlier optical, PET, and MRI studies.

However, despite apparent similarities with other non-invasive imaging modalities, the particular physics associated with MRI modifies many important imaging characteristics relative to other methods. For instance, exogenous contrast agents provide large signal changes associated with CBV by strongly influencing signal in the extravascular space, whereas similarly sized changes in CBV have small effects on PET and CT images that are limited by the small blood volume fraction. Arterial spin labeling can be performed continuously, unlike the PET equivalent using a radioactive label, but quantification of the MRI measurement of CBF is complicated by the rapid decay of the magnetic label.

This chapter focuses on imaging techniques that measure characteristics of the blood supply. A particular emphasis is placed on the use of exogenous contrast agents that enable dynamic measurements of CBV, as this technique is particularly robust and has many connections to blood oxygen level depend (BOLD) signal in terms of both physics and physiology. While BOLD signal is the primary subject of another chapter, it is impossible to discuss CBV techniques without referencing these BOLD connections. Less emphasis is placed on relatively recent methods that employ endogenous contrast mechanisms to assess CBV, as these methods have low

sensitivity and are not yet fully developed. However, CBV measurements using endogenous contrast mechanisms in human subjects possess the potential to inform our understanding of coupling relationships between CBV, CBF, and the cerebral metabolic rate of oxygen utilization ($CMRO_2$). Finally, arterial spin labeling (ASL) has proven to be a very useful tool for interpreting BOLD results and will be briefly discussed.

17.1.1   High-CNR Methods

Because fMRI is a sensitivity-limited technique, the contrast to noise ratio (CNR) per unit time is perhaps the most critical characteristic when assessing alternative fMRI strategies. In general, the most sensitive MRI techniques measure changes in the decay rate of transverse magnetization without limiting these rates through the use of refocusing "spin echoes", as discussed in Sect. 17.2. These signals are derived from blood-borne paramagnetic contrast agents, including agents that are injected into the blood stream or proteins that are contained within the red blood cells.

17.1.1.1   IRON fMRI

Initial fMRI investigations of cerebral physiology and functional activation were performed using bolus injections of contrast agent in animal models (Belliveau et al. 1990b; Rosen et al. 1990) and human subjects (Belliveau et al. 1990a; 1991). Gadolinium chelates, the only contrast agents approved in humans at that time, still are used routinely to assess regional CBF and CBV in the clinic. While such agents produce a strong first-pass effect on MRI signal, rapid vascular redistribution (tens of seconds) followed by removal from the blood (1 h) leave them unsuited for continuous imaging of dynamic changes in CBV. Nevertheless, these studies forecast subsequent dynamic measurements of CBV using contrast agents with an extended blood half-life. Many of the basic features of paramagnetic contrast media for fMRI were first described based upon observations from gadolinium studies.

   The development of superparamagnetic iron oxide blood pool agents (Weissleder et al. 1990) enabled dynamic measurements of CBV in animal models due to ischemia (Hamberg et al. 1996), respiratory challenges (Kennan et al. 1997), and sensory stimulation (Mandeville et al. 1998; Kennan et al. 1998; van Bruggen et al. 1998). In animal models, this technique provides the practical advantage of very high detection power relative to alternative fMRI techniques like BOLD signal (Mandeville et al. 1998; 2004). While we originally referred to this method as "CBV-fMRI", we now employ the IRON moniker – Increased Relaxation for Optimized NeuroImaging (Chen et al. 2001; Mandeville et al. 2004) – to distinguish this technique from T_1-based measurements of CBV and more recently developed methods that do not rely upon contrast agent.

17.1.1.2 BOLD fMRI

Deoxygenated hemoglobin in the red blood cells is a paramagnetic species (Pauling and Coryell 1936) that acts much like exogenous contrast agents, so the physics of BOLD signal has many similarities to the IRON method, although deoxyhemoglobin produces a much smaller blood magnetization than typical iron doses used for fMRI. The physiology of the two methods is very different. While blood magnetization stays quite constant using the IRON method, blood oxygenation changes during a functional challenge, switching the sign of BOLD signal changes relative to IRON fMRI and producing dependencies of BOLD signal on the cerebral metabolic rate of oxygen utilization ($CMRO_2$) and CBF, in addition to CBV.

Oxygen-induced changes in the transverse relaxation rate of blood were reported early in the history of MRI, leading to a conclusion that "the local availability of oxygen in tissues *in vivo* is reflected in T_2 values" (Thulborn et al. 1981; 1982). However, the implications for imaging were unclear. Optical methods soon reported changes in brain function based upon "intrinsic signals", which were thought to contain a contribution "associated with the conversion of oxyhaemoglobin to haeomoglobin in the capillaries" (Grinvald et al. 1986). Ogawa and colleagues measured changes in "blood oxygen level dependent (BOLD) contrast" due to inspired carbon dioxide in rodents (Ogawa et al. 1990a) and speculated that negative BOLD changes would accompany increases in brain activity "resulting from higher oxygen consumption" (Ogawa et al. 1990b). If not for prior PET observations (Fox and Raichle 1986), the speculation of activity-induced negative BOLD signal would have been correct as postulated but for a different reason: if CBF and $CMRO_2$ exhibited the same magnitude of changes during brain activation, blood oxygenation would remain constant so that negative BOLD signal changes would reflect alterations in CBV, as for the IRON method. Most of the following sections focus explicitly upon IRON fMRI but contain supplemental sections to briefly relate how each imaging characteristic relates to the BOLD method.

17.1.2   Low-CNR Methods

Not every aspect of neurovascular physiology can be measured with high detection power, and the IRON method has not been employed in humans due to a lack of approved contrast agents. Techniques that are not routinely employed for fMRI are nonetheless very important for providing information about physiology.

17.1.2.1   ASL

Blood flow is a responsive index of local brain activity that provides the glucose and oxygen to support metabolism. Arterial spin labeling (ASL) is one of the most important tools for assessing brain function by MRI. This method, developed in the early

1990s concurrent with fMRI (Williams et al. 1992; Detre et al. 1992), was employed together with BOLD signal in the earliest human fMRI measurements (Kwong et al. 1992). However, ASL is seldom employed in traditional brain-mapping studies due its low detection power, and clinical appraisals of basal CBF generally use bolus injections of gadolinium, especially for time-critical applications that cannot afford the averaging time required by ASL.

In many ways, ASL is a seductive technique that possesses most of the characteristics that are desirable for functional brain imaging, except for high detection sensitivity. ASL provides reasonably accurate measurements of absolute CBF in most cases, whereas bolus injections of gadolinium only measure relative regional values of CBF or CBV. For activation studies, ASL signals are localized to the microvessels, where most of the magnetically labeled blood water is extracted through the capillaries into the tissue. Despite these advantages, the limited sensitivity of ASL restricts its usage in brain activation studies to a supporting role for the interpretation of BOLD physiology and the assessment of basal physiology.

17.1.2.2   VASO and VERVE

Two recent techniques have begun to explore the possibility of obtaining quantitative indices of CBV without the use of contrast agent, which would extend dynamic functional assessments of CBV physiology into human subjects for the purpose of informing BOLD signal and potentially other aspects of neurovascular physiology. Each of these methods is challenged with the task of interpreting small signal changes in the face of competing contrast mechanisms, but persistent development efforts are beginning to bear fruit. The VASO (vascular space occupancy) method (Lu et al. 2003) may ultimately provide a reasonably robust index of CBV for targeted studies of physiology, whereas the VERVE (venous refocusing for volume estimation) technique (Stefanovic and Pike 2005) targets a more specific biology by attempting to extract the venous contribution to BOLD signal changes.

17.2 T_1, T_2, and T_2* Contrast

If we exclude several contrast mechanisms like diffusion and chemical shifts (NMR spectroscopy) that are discussed in other chapters, fMRI signals *in vivo* result from changes in the relaxation times (T_1, T_2, or T_2*) of water protons as a result of underlying changes in cerebral physiology. Signal changes can occur from endogenous mechanisms like BOLD signal, or from exogenous contrast agents in the blood stream that magnify the sensitivity to changes in vascular physiology. When imaging normal brain with an intact blood–brain barrier (BBB), contrast agents affect brain water somewhat differently than in solution due to compartmentalization of agent within the small cerebral volume fraction contained inside the vessel walls. In brief,

compartmentalization produces the following set of *distinguishing principles* that govern MRI contrast and the technique of choice for particular applications:

1. T_1 contrast agents effect cerebral signal weakly, because the BBB limits exchange of water between the intravascular compartment, containing contrast agent or magnetic labels, and the extravascular compartment, containing the vast majority of water, which is the source of MRI signal.
2. Contrast agents within the blood vessels produce magnetic field gradients that extend into the extravascular tissue. Using T_2^* weighting of signal, all water protons in the brain are effected by intravascular agent, so that the influence of CBV on MRI signal is magnified. T_2^* includes effects that would be removed by the use of spin echoes, so changes in T_2^* always exceed changes in T_2.
3. When using spin echoes to refocus magnetic field inhomogeneities, extravascular water protons are strongly influenced only in the vicinity of microvessels, where magnetic field gradients change rapidly on a spatial scale comparable to the diffusion length. Hence, spin echoes improve microvascular weighting but sacrifice a significant portion of the available signal near larger vessels.

To elucidate upon the first point above, the rate of exchange for water across the BBB is comparable to T_1 values of the brain (Donahue et al. 1996). During the time that longitudinal magnetization recovers backs to equilibrium, only a small fraction of water protons in the extravascular space are subjected to cross-relaxation by close contact with water that initially relaxed at a different T_1 rate due to the presence of contrast agent. As a consequence, the volume fraction of spins that participates in modifying the MRI signal due to a change in CBV is very limited using T_1 methods. For instance, consider a robust functional stimulus (e.g., strong visual stimulus) that produces a 25% increase in CBV; assuming a 4% basal blood volume fraction in the tissue region responding to the stimulus, only about 1% of the total brain water is displaced by blood water carrying additional contrast agent. Hence, only about 1% of the MRI signal (plus a small additional amount due to transvascular water exchange) senses the additional contrast agent. For this reason, T_1 agents aren't useful for fMRI. Conversely, the low sensitivity of cerebral MRI signal to T_1 agents within the vasculature is a benefit for imaging breakdown of the BBB in pathology, a case where T_1 effects are visualized easily due to extravasation of agent into the extravascular space (Zaharchuk 2007).

In contrast to longitudinal signal, transverse signal requires spin coherence across an image voxel, and this coherence can be disrupted *at a distance* by magnetic field gradients that extend outside the vessels. This effect was postulated (Villringer et al. 1988) based upon physical principles and a very simple observation: the signal attenuation observed in their studies (50%) due to injection of gadolinium into rat brain far exceeded the blood volume fraction, implicating an extravascular source. In fact, the signal to noise ratio (SNR) of gradient-echo sequences can be driven to zero in animal models by injecting large doses of agent, showing that all water protons in the brain are subjected to the magnetic gradients that extend outward from vessels.

From the earliest uses of exogenous agent *in vivo*, it was apparent that gradient echoes and spin echoes produced qualitatively different contrast: gradient echoes

Fig. 17.1 Simulations of gradient-echo (R2*) and spin-echo (R2) relaxation rates versus vessel diameter indicate that gradient echoes have no sensitivity to vessel size, whereas spin echoes are preferentially sensitive to microvessels but have much less overall sensitivity
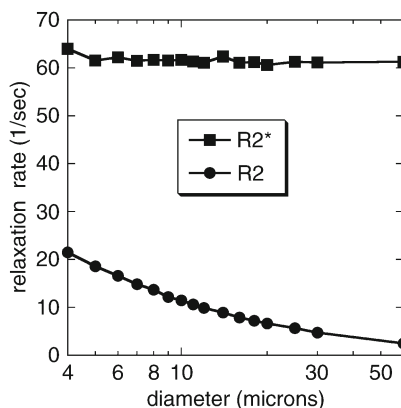
showed more signal attenuation per unit dose throughout the brain, and differences were particularly pronounced near large vessel regions. Spin-echo measurements were hypothesized to most strongly reflect signal around capillaries (Fisel et al. 1989; Rosen et al. 1991). Given that spin echoes refocus effects of time-independent magnetic field variations, the physics behind the strong capillary weighting for spin-echo measurements is straightforward. In the absence of water diffusion, a spin echo would refocus all phase variations across a voxel, but random field variations sampled by water molecules during diffusion are not refocused. During the few tens of milliseconds over which the NMR signal is sampled during T_2 decay, the average displacement due to water diffusion is no more than a few tens of microns. In order for the magnetic field to produce meaningful changes to the phase of a diffusing water molecule, field variations must occur on a microscopic scale comparable to the diffusion distance. Magnetized vessels produce external magnetic fields with (1) a radial dependence that drops off with a distance comparable to the vessel size, and (2) a strong angular dependence. These dipolar field dependencies implicate microvessels with sizes less than or comparable to the diffusion scale as the dominant sources of signal change when using spin echoes. Conversely, magnetic fields near large vessels appear to be almost static (time-invariant) in the frame of a diffusing water molecule. Near such vessels, phase increments acquired prior to the inversion pulse are reversed and then unwound by the time signal is acquired, so large vessels produce small effects on spin-echo signal.

We can simulate the dependence of relaxation rates upon vessel size for both spin echoes and gradient echoes using standard Monte Carlo methods (Boxerman et al. 1995b). Figure 17.1 shows relaxation rates for a hypothetical voxel containing a physiological CBV distributed in randomly oriented but fixed-diameter vessels, each containing a concentration of contrast agent that would result from systemic injection of about 15 mg of iron per kg of body weight. At such high blood magnetization, gradient-echo measurements have no sensitivity to vessel size, so signal changes can be quantitatively related to total CBV.

Using spin echoes, contrast agents produce the largest influence on MRI signal near the smallest microvessels, and the effect then decreases monotonically with

vessel size, as shown in Fig. 17.1 (Mandeville et al. 2007a). This basic dependence, suggested prior to fMRI using exogenous or BOLD contrast (Rosen et al. 1991), underlies claims that spin echoes are preferentially sensitive to microvessels. The strong vessel-size dependence of spin-echo measurements of CBV motivated "vessel size imaging", in which a mean vessel size index can be formed from the ratio of gradient-echo and spin-echo measurements (Dennie et al. 1998; Tropres et al. 2001). The potential advantages, and the clear disadvantages, of spin echoes for fMRI will be discussed later.

17.2.1 BOLD Connection

There are qualitative connections between the simulations of Fig. 17.1 and BOLD signal. At lower levels of blood magnetization appropriate for BOLD signal or for FDA-approved doses of gadolinium, gradient echoes exhibit less sensitivity to capillaries than to larger vessels (Boxerman et al. 1995b). Even at such low levels of blood magnetization, spin echoes are preferentially sensitive to microvessels, and this sensitivity becomes progressively more pronounced as blood magnetization increases (Boxerman et al. 1995b). However, assumptions about vessel size dependencies using either gradient or spin echoes for BOLD imaging should be entertained with caution, as a significant proportion of BOLD signal occurs within the intravascular compartment, particularly at clinical field strengths (Boxerman et al. 1995a; Song et al. 1996). At higher fields, intravascular contributions are reduced for a given echo time, but increased susceptibility artifacts at high field generally force the use of shorter echo times, so that intravascular BOLD contributions remain at high fields. Spin echoes, which are insensitive to susceptibility artifacts, are dominated by intravascular signal at low field (Zhong et al. 1998; Oja et al. 1999), but very high fields like 9.4 T eliminate the intravascular contribution even without using extraordinarily long echo times (Lee et al. 1999). However, spin echoes suffer a multi-fold loss of detection power relative to gradient echoes, a major drawback at any field strength.

17.3 IRON fMRI

17.3.1 Interpretation of T_2 and T_2^* Changes

Although it is common in radiology to speak of MRI contrast in terms of relaxation times, quantitative models are constructed with the inverse quantities, which are rates: $R_2 = 1/T_2$. Several approximations simplify the math. The first is that relaxation rates are additive ($R_2^{TOTAL} = R_2^{ENDOGENOUS} + R_2^{AGENT}$), an assumption that requires a single compartment. This is not strictly true, because the intravascular and

extravascular compartments are separated by slow exchange on the scale of the echo time. When agent is first injected into the blood stream, signal from the small intravascular compartment is nulled, leaving only the extravascular compartment as a source of subsequent functional signal changes. However, so long as doses of contrast agent produce sufficiently large changes in MRI signal, the small intravascular compartment can be ignored. A second assumption is that contrast agents increase relaxation rates in proportion to the tissue concentration of contrast agent ($R_2^{AGENT} = k\,C$), where C is the tissue concentration of agent (Rosen et al. 1990). This is a useful concept in terms of connecting bolus infusions, where the time dependence reflects changes in the intravascular concentration of agent at a fixed volume fraction ($R_2^{AGENT}(t) = k\,C_{BLOOD}(t)\,V_0$), to the use of steady-state blood pool contrast agents, where the time dependence reflects dynamic changes in blood volume ($R_2^{AGENT}(t) = k\,C_{BLOOD}\,V(t)$). However, simulations suggest a slightly superlinear dependence of relaxation rate upon blood concentration at very low levels of blood magnetization with a linear dependence upon the blood volume fraction (Boxerman et al. 1995b); the latter dependence is all that matters for IRON fMRI, as long as the blood concentration remains constant.

With these two assumptions in place, MRI signal changes can be related to percentage changes in CBV using the IRON method. Upon injection of contrast agent, a new relaxation process attenuates the signal with a proportionality to the basal blood volume fraction: $R_2^{AGENT}(t=0) = k\,V(0)$. Subsequent functional changes in blood volume are reflected in time-dependent changes in this relaxation rate, $R_2^{AGENT}(t) = k\,V(t)$, such that changes in MRI signal can be directly related to percentage changes in the blood volume fraction, $\Delta V(t)/V$, by normalizing functional responses to the effect produced by injection.

In this formulation, we ignored two additional potential influences on MRI signal: T_1 effects and BOLD signal. As described previously, transvascular water exchange across an intact BBB is slow, so T_1 effects can be ignored even when large doses of contrast agent are used or when the repetition time is short. During a functional response, the BOLD mechanism competes with IRON signal. For a typical sensory stimulus, for instance, BOLD signal changes are positive and IRON signal changes are negative, so changes in relaxation rates oppose each other: $\Delta R_2(t) = \Delta R_2^{IRON}(t) - \Delta R_2^{BOLD}(t)$. Typically, BOLD contamination in IRON signal enters at a level of only 10–20% even at high fields like 9.4 T in animal models (Mandeville et al. 2004), although this may overestimate BOLD effects because the intravascular part of BOLD signal is crushed upon injection of agent, leaving only the extravascular BOLD effect to compete with IRON signal changes. Empirically, drug-induced changes in CBV were found to be quite consistent across a fivefold range of magnetic field when ignoring BOLD effects (Mandeville et al. 2004).

The ability to quantitatively measure a relatively interpretable physiological index (the activation-induced percentage change in CBV using gradient echoes) is a significant advantage of IRON fMRI when juxtaposed relative to the complexities of BOLD signal. IRON results can be compared directly to other modalities that report changes in CBV or CBF (which can be related to CBV), and there is little dependence of this index on magnetic field strength.

The preceding discussion cannot be applied to spin echoes without accounting for the vessel profile shown in Fig. 17.1. When vessels swell, they become less effective at relaxing MRI signal. Hence, relaxation rate ratios systematically underestimate actual percentage changes in microvascular CBV. If we assume that all vessels respond similarly to a stimulus, simulations find that spin-echoes underestimate actual changes in CBV by about 30–40%, and this prediction roughly matches data across most of the brain (Mandeville et al. 2007a). Of course, vessels do not all respond similarly, so model-independent quantification of the percent changes in microvascular CBV is not possible.

17.3.1.1   BOLD Connection

Deoxygenated hemoglobin is a paramagnetic species (Pauling and Coryell 1936; Thulborn et al. 1982; Ogawa and Lee 1990) that acts much like exogenous contrast agents, so BOLD models start from the same perspective described above. However, there are several important differences that complicate quantification of BOLD signal or comparison of BOLD signal across studies.

Firstly, BOLD signal contains an intravascular contribution that generally is dominant at low fields like 1.5 T and progressively diminishes with higher fields. This intravascular contribution can be separated explicitly from extravascular signal or swept up into an effective relaxation rate that has a superlinear dependence upon blood magnetization (Buxton et al. 2004). The relative contribution of intra/extravascular effects is a complicated function of magnetic field strength and echo time.

Secondly, one cannot simply determine the baseline BOLD relaxation rate, which is entangled with other endogenous relaxation processes. Using exogenous agents, the baseline relaxation rate is determined by observing signal attenuation due to injection of agent. There is no analogous method for BOLD signal. An indirect way to determine the baseline BOLD effect is a method that requires inhalation of CO_2 together with combined measurements and BOLD signal, CBF, and optionally CBV (Davis et al. 1998; Mandeville et al. 1999a). Thus, there is no way to routinely compute a physiological index analogous to the IRON method (i.e., the percentage change in deoxygenated hemoglobin). Given these problems with quantification, literature studies typically quote purely statistical quantities, or they report percentage changes in BOLD signal, a quantity that is related to absolute changes in deoxygenated hemoglobin but that has multiple complicated dependencies on specific experimental parameters and the underlying basal physiology.

17.3.2   Detection Power

Detection power generally governs the choice of alternative fMRI strategies. Consider, for example, how rarely ASL is used within the brain mapping community in relation to BOLD signal. Despite the numerous reasons in principle to choose

ASL over BOLD signal (e.g., less uncertainty in terms of interpreting the response, ability to assess the basal physiological state, signal changes more localized to microvessels), the larger CNR of BOLD signal trumps all other arguments, leaving ASL as a niche technique in the fMRI community (albeit an important one).

Similarly, the CNR advantages for IRON fMRI in animal models are so pronounced at typical field strengths that most animal studies would benefit enormously by using exogenous agent in place of BOLD signal. At low magnetic fields like 1.5 or 2 T, IRON boosts CNR relative to BOLD signal roughly sixfold (Mandeville et al. 1998; Vanduffel et al. 2001). Averaging increases CNR only in proportion to the square root of time, meaning that low-field BOLD fMRI requires about 30-fold more averaging to obtain similar results. At higher MRI fields strengths, BOLD detection power improves due to the linear scaling of deoxyhemoglobin magnetization with field strength. At 9.4 T and higher, BOLD signal is much more competitive (within a factor of 2 of IRON CNR), with the comparison depending upon details of the methodology (Mandeville et al. 2004; Zhao et al. 2006).

There are many avenues for improving the absolute CNR in any experiment by increasing the SNR. Because the strongest influence on SNR is the voxel volume, spatial resolution generally is purchased at the expense of detection power. Obviously, this argument falls apart when voxels exceed the size of a focal activation, so that detection power is limited by volumetric dilution of the response. Additionally, physiology and motion contribute noise sources that scale with the magnitude of signal (Kruger and Glover 2001; Kruger et al. 2001; Triantafyllou et al. 2005). When the SNR in individual images exceeds a value of about 100, further improvements in image SNR do not translate to the temporal domain (Triantafyllou et al. 2005). In this regime, CNR does not decrease as much as SNR when voxels become smaller or (presumably) when contrast agent is injected.

Using the IRON method, detection power relative to BOLD signal depends upon a number of considerations that often are counter-intuitive. For instance, contrast agents decrease SNR but increase CNR; detection power for BOLD signal is much more sensitive to basal CBV than IRON signal; the best results using the IRON method are obtained at very short echo times; percentage changes in IRON signal are insensitive to the MRI field strength; the relative ratio of BOLD and IRON CNR depends upon the duration of the applied stimulus. The following sections elaborate upon these points.

17.3.2.1 Echo Time and Dose

To optimize detection power using T_2*-based contrast for fMRI, one always sacrifices SNR for the sake of CNR. Using BOLD signal, for instance, echo times near zero achieve maximal SNR, whereas echo times close to tissue T_2 or T_2* maximize CNR at a much lower SNR. This same principle holds true when using IRON fMRI. At any given echo time, the dose of contrast agent should be adjusted so that SNR falls to about 1/e of the pre-injection value. However, IRON fMRI presents experimenters with the opportunity to adjust two experimental knobs: echo time and dose.

Fig. 17.2 In the two-dimensional space of echo time and contrast agent dose, where dose in the figure is indicated by the effect on the transverse relaxation rate of MRI signal, the functional contrast to noise ratio (CNR) is optimized at short echo times and large doses of contrast agent
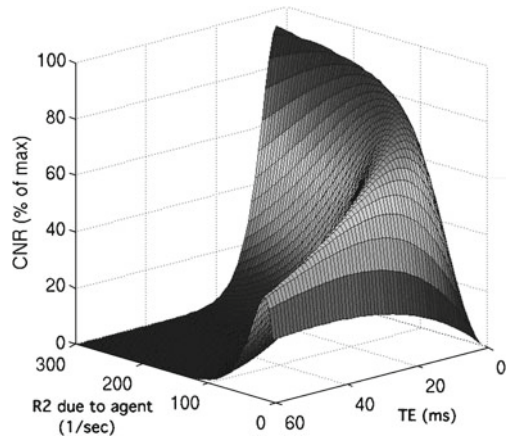
In this two-dimensional space, shown in Fig. 17.2, there is a global maximum of CNR corresponding to an unattainable solution: zero TE and an infinite dose of contrast agent.

Fortunately, lengthening the echo time has only a modest effect on the maximum available post-injection CNR, which scales in proportion to the pre-injection SNR as $\exp(-T_E/T_2^*)$. Setting the echo time to $T_2^*/2$, for instance, delivers about 60% of the maximum possible signal change. In animal models where dose limitations are not a concern, short echo times can be used to produce the best possible set of imaging characteristics: large signal changes, minimal susceptibility artifacts, and many slices or excitations per unit time. At high field strengths like 9.4 T, where the T_2^* distribution has a large dispersion relative to lower fields, short echo times can make images insensitive to magnetic susceptibility artifacts, while still delivering excellent detection power by suitably adjusting the dose of contrast agent (Mandeville et al. 2004).

To understand typical agent doses and the corresponding relaxation rates induced by injection in animal models, consider the following examples. For repeated fMRI in non-human primates at 3 T, we typically employ single-shot EPI with echo times in the range 20–25 ms and contrast agent doses of 10–12 mg iron per kg body weight. In these studies, the agent-induced relaxation rate is typically 25–30 1/s (Leite et al. 2002). For pharmacological fMRI using multi-shot imaging at 9.4 T in rodents, we employ very short echo times (5 ms) with very large iron doses (35–40 mg/kg) corresponding to iron-induced relaxation rates of about 150 1/s (Mandeville et al. 2004).

As a "rule of thumb" for determining agent dose, global cerebral signal should be attenuated by about a factor of 2 relative to the pre-injection baseline signal at any echo time. In that case, the brain will exhibit a distribution of signal attenuations similar to that shown by the gray curve in Fig. 17.3 (gray matter corresponds to values greater than about 0.5 on the x axis), so that there is little variation in detection power across the brain.
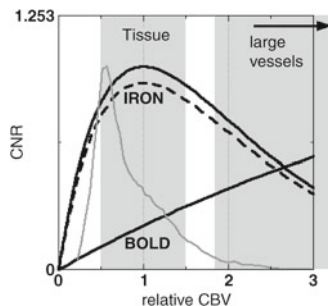
Fig. 17.3 Empirically informed CNR calculations for BOLD and IRON fMRI at 3 T are plotted versus the relative basal blood volume fraction, which is calculated as $rCBV = -\ln(S_{POST}/S_{PRE})$, where S_{POST} and S_{PRE} correspond to signal values prior to and after injection of an exogenous iron oxide blood pool agent. The *dotted line* shows the influence of BOLD contamination in IRON signal. Calculations ignore the different temporal responses and so are appropriate for very long stimuli. The *solid gray line* shows an empirical distribution of basal blood volume as measured in a rat (Mandeville et al. 2007a). Values of rCBV below 0.5 correspond roughly to white matter

17.3.2.2   Blood Volume Fraction

Figure 17.3 shows IRON CNR as a function of basal CBV, with and without inclusion of the concomitant BOLD effect at 3 T. The abscissa in the figure is the relative basal blood volume fraction (rCBV), defined according to the signal attenuation produced by injection of contrast agent: $rCBV = -\ln(S/S_0)$, where S_0 is the pre-injection signal; of course, rCBV is a relative index that is proportional to echo time and dose using this formulation. This index of rCBV is similar to the index used in human clinical studies, where rCBV represents the integral of the regional response profile of the agent-induced relaxation rate following injection of gadolinium. The main difference is that the definition employed in Fig. 17.3 is not normalized by the echo time in order to create a relaxation rate. This definition is convenient for IRON fMRI, because an rCBV value of unity corresponds to the dose and blood volume fraction where detection power is optimal irrespective of the echo time used in the study.

The IRON curves in Fig. 17.3 result from the product of decreasing SNR and increasing percent signal changes versus rCBV: $CNR \sim rCBV \cdot e^{-rCBV}$. Of course, rCBV is regionally variable in the brain, so CNR cannot be optimized simultaneously for all values of rCBV. However, there is little variation in CNR versus the basal blood volume within a physiological threefold range across brain regions (Mandeville and Marota 1999). The gray line in the figures shows an empirical distribution of gradient-echo rCBV from a recent study by our group in a rat (Mandeville et al. 2007a). Values of rCBV below 0.5 in the figure correspond almost exclusively to white matter. When an appropriate dose of contrast agent is employed, tissue CNR is high and large vessel regions are suppressed. These calculations have been validated empirically across a fivefold range of magnetic field strengths by comparing the ratio of IRON and BOLD CNR versus the basal blood volume fraction (Mandeville et al. 2004).

17.3.2.3 Magnetic Field

Unlike BOLD signal, where blood magnetization is a function of the strength of the magnetic field, the relative signal changes for IRON fMRI have no field dependence aside from the small effect of BOLD contamination. Using a theoretical paramagnetic exogenous contrast agent, dose would be adjusted at each field to achieve the desired signal attenuation, as previously described. The available contrast agents that are most suited to the IRON technique are coated iron oxides like MION (Weissleder et al. 1990) and Feraheme (Coyne 2009). Iron oxides are superparamagnetic, which means that the induced blood magnetization has almost no dependence on field strength above 1.5 T (Shen et al. 1993). Hence, a given dose produces the same effect on MRI signal regardless of field strength.

17.3.2.4 Stimulus Duration

Following stimulation, the time for CBV to reach a maximum response is much longer than for CBF or BOLD signal, as described in more detail in the following section. Thus, the size of the CNR boost relative to BOLD or ASL techniques depends upon the duration of the applied stimulus. For instance, CNR enhancement relative to BOLD signal drops to about a factor of 2 when using short stimuli (e.g., 4 s) that are appropriate for event-related fMRI at 3 T (Leite et al. 2002). A poorly constructed event-related paradigm using periodic stimuli with a short inter-stimulus interval would see a further big loss of CNR due to the low-pass filtering of the slow IRON response. However, randomizing the inter-stimulus interval alleviates any loss of CNR due to overlap of adjacent stimuli (Leite and Mandeville 2006), in the same way as for BOLD signal (Burock et al. 1998). Because the IRON response is slower than the BOLD response, it is even more crucial that event-related stimuli be randomized in time.

BOLD Connection

The physics of BOLD extravascular signal is identical to that for the IRON method, except that blood magnetization generally is much lower. If a very low dose of iron oxide were employed in an experiment, the relationship between CNR and the basal blood volume fraction would be similar to that shown for BOLD signal in Fig. 17.3. When blood magnetization is low enough that regional variations in CBV are not evident in individual images (e.g., the exponential dependence of CNR on SNR is weak), CNR will increase with an almost linear dependence on the basal blood volume fraction. In this contrast-starved regime that is typical for BOLD images, functional responses are much more easily observed in large vessel regions such as draining veins and the superficial layers of cortex (Mandeville and Marota 1999; Zhao et al. 2006). This creates a "brain versus vein" localization problem that is not an issue for IRON fMRI. Note that this argument does not require significant levels

Fig. 17.4 BOLD (*open circles*) and IRON (*closed circles*) data in macaque visual cortex using stimuli of duration 2, 4, 16, and 32 s show the pronounced effect of stimulus duration on IRON signal
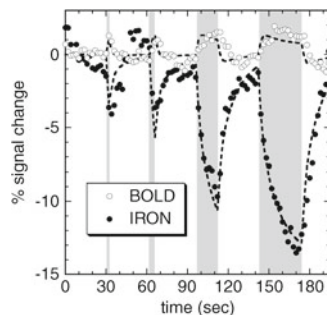
of BOLD intravascular signal, which provides a valuable additional source of signal changes but exacerbates the brain-versus-vein conundrum. Loss of spatial localization due to venous drainage of deoxygenated hemoglobin during a stimulus is an effect that is observed not only in large veins, but in regions that bridge activated tissue and large veins (Leite et al. 2002). This effect does not go away at high magnetic fields like 9.4 and 11.7 T (Silva et al. 2007).

17.3.3 Temporal Response

Following our initial observation that CBV responds much more slowly than BOLD signal following a functional stimulus (Mandeville et al. 1998), we compared the temporal responses of CBF and CBV using very high temporal resolution in order to additionally detect the rapid phase of the CBV response that accompanies arterial dilation and the rapid onset of CBF. In fact, CBV initially responds as rapidly as CBF (Mandeville et al. 1999b) and more rapidly than BOLD signal (Marota et al. 1999; Silva et al. 2007), which is delayed by the washout nature of the technique. Prolonged stimulation produces a continued slow rise of CBV with a minimal influence on CBF. Following cessation of stimulation, CBF resolves to baseline more quickly than CBV, which does not return to baseline for 30–60 s. These temporal dynamics for the IRON response now have been observed in many rodent studies (Mandeville et al. 1999b; Lu et al. 2005; Silva et al. 2007; Kida et al. 2007) and in awake non-human primates (Vanduffel et al. 2001; Leite et al. 2002). The IRON response is amenable to a linear model analysis using a hemodynamic response function that contains both a rapid and a slow temporal component (Leite et al. 2002; Leite and Mandeville 2006; Silva et al. 2007).

Figure 17.4 shows typical BOLD and IRON responses in the visual cortex of an awake non-human primate in response to a visual stimulus of variable duration. The response is the summation over all image voxels that were significantly correlated with the stimulus using both methods. During the two longest stimuli (16 and 32 s), the BOLD response reaches a plateau, whereas the IRON response continues to grow.
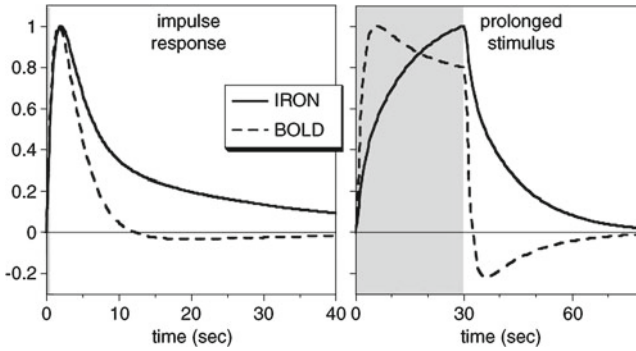
Fig. 17.5 Left: Impulse response functions for IRON and BOLD signal in macaque visual cortex. Right: The response to a long stimulus is predicted by convolving the impulse response with a square function indicating the stimulus timing. For extended stimuli, the slow evolution of IRON signal is more apparent, and BOLD signal shows a pronounced post-stimulus undershoot

As a practical matter of data analysis, the main difference between the BOLD and IRON hemodynamic impulse response functions (IRF) is that sign of the tails are switched (Leite et al. 2002). For a short stimulus, BOLD signal increases with a rapid onset time and then decreases slightly below the baseline level for several tens of seconds after the end of stimulation, as shown in Fig. 17.5 (left). For very short stimuli, the post-stimulus undershoot is a subtle effect that is not detected in all experiments. The response to longer stimuli can be approximately predicted by time-shifted summation of the IRF (Boynton et al. 1996), or alternatively by convolving a parametric IRF with the stimulus timing. For a much longer stimulus (Fig. 17.5, right), the result is a more pronounced post-stimulus undershoot due a slow build-up of the negative tail. The IRON response depicts the same general features, except that (1) the tail of IRF does not switch sign as in the BOLD IRF, and (2) the tail of the IRF is a much more prominent feature in the IRF, so the slow component of the IRON response dominates for extended stimuli. These features of the response also are manifest in more complicated experimental designs using rapidly presented event-related stimuli. For such stimuli, the tail of the IRON response builds into a pronounced offset of the average signal level relative to non-stimulated states, whereas the BOLD tail counteracts baseline shifts that would be otherwise observed (Leite et al. 2002; Leite and Mandeville 2006).

Mathematically, the response of CBV can be simulated by adapting the windkessel concept that is used to describe the compliance of larger arteries in response to periodic pressure waves produced by the heart. In the windkessel formulation (Mandeville et al. 1999b), arteriole dilation in response to a functional stimulus increases intravascular pressure downstream, and this generates dilation of capillaries and venules due to the compliant nature of those vessels. Dilation can be either elastic, meaning that vessels respond rapidly like a balloon, or inelastic due to the presence of an additional physical process with a longer time constant. Due to the biphasic nature of the CBV response, as well as optical experiments that suggest a rapid

response of total hemoglobin volume in the capillary compartment, we proposed elastic dilation followed by inelastic expansion of vessels for prolonged stimuli, or "delayed compliance". Optical and fMRI studies using short stimuli have applied or extended this model to accurately describe data for stimuli of short duration without invoking an inelastic response (Friston et al. 2000; Boas et al. 2008), whereas other optical investigators have expanded upon the delayed compliance model by replacing our original ad hoc approach to the inelastic phase with a state variable to govern inelastic dilation (Kong et al. 2004). Within the "balloon" framework for BOLD signal (Buxton et al. 1998b), the CBF-CBV temporal relationship has been modeled using identical equations (Buxton et al. 2004) with a single long time constant, which has the effect of stretching the mean transit time; this approach might be viewed as a purely inelastic model for slow capillary/venous dilation which views the rapid phase in the data as solely due to arterial dilation. Potential mechanisms underlying this response are discussed at the end of the chapter.

17.3.3.1   BOLD Connection

Our data has shown that the temporal mismatch observed between the dynamic responses of CBF and CBV contributes to the BOLD post-stimulus undershoot. Following cessation of electrical forepaw stimulation in rats, the undershoot begins when percent CBF falls below percent CBV, and the undershoot resolves when CBV resolves to baseline (Mandeville et al. 1999a). Using a linear model analysis of fMRI data from the visual cortex of awake non-human primates (Leite et al. 2002), two temporal components were identified that could consistently fit both the CBV and BOLD data in multiple stimulus presentation designs using relative magnitudes that were physiologically reasonable; the CBV response was more heavily weighted by the slow (capillary/venous) response than the fast response, and the influence of CBV (slow response) in BOLD signal was only about one third as large as the influence of blood oxygenation (fast response). Alternate hypotheses about BOLD temporal dynamics are discussed in the last section.

Figure 17.6 compares the integrated amplitude of the BOLD and CBV responses in rat somatosensory cortex during a post-stimulus 20-s window that was delayed by 7 s relative to stimulus cessation (Royl et al. 2001). As a function of stimulus duration, the BOLD undershoot becomes larger, together with the average magnitude of CBV, which has a negative influence on BOLD signal.

Is it possible that the BOLD and IRON responses have such an excellent anti-correlation in the post-stimulus temporal region because the BOLD post-stimulus undershoot is producing an artifact in the IRON response? In other words, could elevated oxygen utilization or a flow undershoot in the post-stimulus region produce elevated levels of deoxygenated hemoglobin, which would add to the negative IRON signal and make it appear that the response was delayed? This potential artifact cannot explain the data. Consider the non-human primate of Leite et al. (2002). Changes in iron-induced relaxation rates were about seven times larger than BOLD changes at the end of a prolonged stimulus, so the BOLD effect is a minor correction to the

Fig. 17.6 The integrated amplitude of MRI signal during the post-stimulus region for BOLD signal and CBV shows that the magnitude of the BOLD undershoot correlates with the post-stimulus response of CBV, which has a negative effect on BOLD signal (Royl et al. 2001)
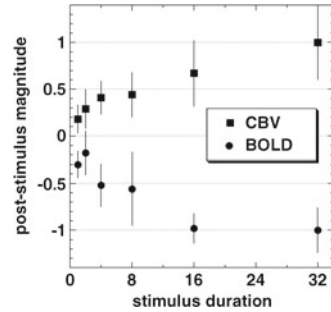
IRON response in most circumstances. Moreover, when the BOLD post-stimulus undershoot began about 10 s after stimulus cessation, the IRON-induced relaxation rate was still about three times larger than the maximum positive BOLD response at any time point. In other words, the BOLD effect simply is not strong enough to significantly alter the temporal dynamics of the IRON response when appropriate doses of contrast agent are employed.

Although IRON signal initially responds more rapidly than BOLD signal (Silva et al. 2007), it is fair to say that the IRON method suffers a loss of temporal resolution as compared to BOLD signal, meaning that the slower time-to-peak for the CBV response leads to a greater relative loss of CNR using short or rapidly presented stimuli compared to longer block designs for stimulation.

17.3.4   Spatial Resolution and Localization

Relative to the spatial resolution defined by neuronal ensembles responding to as stimulus, fMRI suffers a loss of spatial resolution that can be understood as convolution with a vascular point spread function (PSF) that introduces blurring (Engel et al. 1997). The 2-deoxyglucose technique revealed that the metabolic response to visual stimuli in macaque visual cortex can be as small as a few hundred microns or less, depending upon the cortical layer (Tootell et al. 1988). However, the ultimate spatial resolution obtainable by fMRI remains somewhat controversial. This issue is confounded by large differences in detection power between alternative methods, by hardware limitations, and by other experimental details.

There have been several oft-cited attempts to define a PSF for fMRI using retinotopy (Engel et al. 1997; Parkes et al. 2005; Shmuel et al. 2007), each reporting a PSF of several millimeters. Not coincidentally, these estimates correspond roughly to the size of the imaging resolution in these studies. Such studies do not probe the "intrinsic" resolution of fMRI, but rather demonstrate the constraints of hardware and techniques employed in typical fMRI studies.

Figure 17.7 illustrates that higher spatial resolution can define a smaller PSF. In this study in awake macaques (Leite et al. 2005), we used isotropic 1.25 mm voxels and parametrically varied the size of small point-like stimuli in order to estimate the

Fig. 17.7 Data show measured full width at half maximum of retinotopic projections of point-like stimuli using IRON fMRI. The solid line fits the data, and the dashed line removes the combined effects of the pixel resolution and T2* blurring to estimate the sum of the neuronal and vascular spreads (Leite et al. 2005)
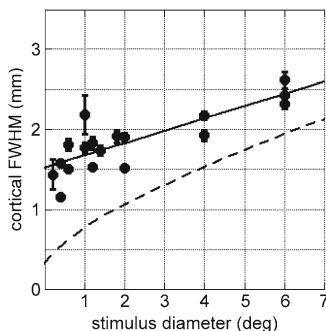
retinotopic projection of a vanishingly small stimulus, which should correspond to a neuronal response with a minimal spatial spread. As seen in the figure, gradient-echo IRON fMRI can directly measure a spatial spread of no more than 1.5 mm. When one accounts for the finite size of imaging voxels and the blurring function induced by the T_2* decay filter across the spectrum of spatial frequencies during data acquisition, the "intrinsic" point spread of fMRI is projected to be well less than a millimeter (dotted line), and probably just a few hundred microns (Leite 2006).

In addition to spatial resolution, which is a measure of the width of a focal response, spatial localization can be defined as the foci (or centroid) of a response. In turn, localization has aspects that depend upon both the physiology and the physics of a technique. As an example of the differentiation between physiology and physics, consider how ASL can be subtly differentiated from flow. The net flow of blood through the veins is identical to that in arteries and capillaries, and yet very little of the magnetic label for ASL survives into the veins due to water extraction in the capillaries. Hence, small shifts between BOLD and ASL signals will be observed due the venous and capillary weightings, respectively, for the two methods.

The spatial foci of IRON and BOLD fMRI also differ subtly for reasons that largely can be defined from the physics of the methods. BOLD signal has a much stronger dependence on basal CBV, as seen in Fig. 17.3. Regions with high basal CBV exhibit a larger BOLD/IRON signal ratio than regions with low basal CBV, and this is generally true across whole brain (Mandeville et al. 2001). Cortical laminae exhibit a strong gradient of basal CBV that increases toward the superficial layers, and so a focal cortical response due a sensory stimulus produces a BOLD activation pattern that is amplified in superficial cortical layers relative to the IRON response, which is largest in middle cortical layers (Mandeville and Marota 1999; Zhao et al. 2006). In species with cortical folds like non-human primates, the IRON response in sulci can be more easily localized to a specific cortical bank, because the superficial weighting of BOLD signal brings the response centroid near the convergence of the two cortical surfaces (Vanduffel et al. 2001).

The precise spatial relationship between neuronal and fMRI responses is unclear. Some authors have speculated that localization of the CBV response to the middle cortical layers might represent "laminar specificity" for localizing neuronal responses by fMRI (Harel et al. 2006). Alternatively, combined spin-echo and gradient-echo measurements of CBV show that superficial layers of cortex have a

higher basal blood volume fraction and a larger mean vessel size than middle corti-cal layers, suggesting that large but less reactive conduit vessels diminish CBV reactivity near the cortical surface (Mandeville et al. 2007a). Although it is possible and even probably that fMRI eventually will distinguish differential neuronal responses across cortical laminae, there is not yet evidence for this.

17.3.4.1   BOLD Connection

Results are shown for IRON fMRI in Fig. 17.7, but we obtained virtually identical results for BOLD fMRI. fMRI experiments in humans with an isotropic resolution approaching 1 mm will soon be routine as a result of advances in gradient strength technology and parallel imaging, which extend the range of k-space that can be sampled per unit time, and due to the proliferation of higher magnetic field strengths (particularly 7 T), which support higher resolution through a higher intrinsic SNR.

17.3.5   *fMRI in Animal Models: Choosing a Technique*

There are many disparate reasons for performing fMRI in animal models. Some investigations target specific aspects of physiology or functional coupling (e.g., mechanisms of BOLD signal) and might choose methods less based upon efficacy than on the specific biological information that can be obtained. Another class of experiments – let's call it "brain mapping" – seeks neural correlates related to behavior, state, or stimulus parameters with the presumption that different aspects of the vascular response (CBF, CBV, BOLD signal) provide essentially the same information in terms of neural coupling. Example applications in this class include drug infusions to investigate specific neurotransmitter systems or neuronal plastic-ity resulting from prolonged drug exposure, sensory stimulation to provide neural correlates of functional recovery following stroke (Dijkhuizen et al. 2003), and investigations of normal sensorimotor/cognitive processing for comparison with human subjects (Tsao et al. 2003) or as the basis for targeted electrophysiological studies (Tsao et al. 2006).

Animal models present an inherent set of difficulties that is beyond the scope of this chapter. The main issues, of course, are anesthesia or motion. Anesthesia blunts the size of signal changes, most generally by inhibiting synaptic transmission but also by shifting vascular baseline physiology. In conscious animals, signal changes may be larger, but noise also is larger due to brain or body motion; the latter produces appar-ent brain motion by inducing time-dependent changes in the magnetic field. Effective fMRI requires significant attention to the biological/behavioral aspects of an animal model, as well as an understanding of the available fMRI methods. Generally, experi-menters desire not only to detect functional changes in obvious regions (e.g., primary sensory cortex) but in higher or connected regions as well, and then to somehow manipulate those responses through stimuli or pretreatment. Obviously, bigger signal changes are better when choosing an fMRI contrast mechanism.

With these considerations, most fMRI applications in animal models come down to a choice between BOLD or IRON signal. At field strengths below 5 T, the IRON method always provides a large CNR gain over BOLD signal. At field strengths approaching 10 T, the choice is more complex. For imaging the effects of drugs, high-resolution whole-brain imaging is desirable with less emphasis on rapid image collection due to the slow evolution of the neural response. In such a case, multi-shot sequences can be employed with short echo times (5 ms) to cover whole brain with minimal susceptibility artifacts at high fields while providing all of the IRON benefits of higher tissue CNR and lower signal from draining venous sinuses. For sensory stimulation studies at 9.4 T, two factors combine to reduce IRON CNR and make the BOLD/IRON comparison virtually a wash in terms of CNR (Zhao et al. 2006): rapid single-shot imaging is beneficial for CNR but requires a somewhat longer minimal echo time (10 ms), and the slower temporal evolution of CBV decreases IRON CNR for short stimuli. The first consideration eventually will be removed by hardware improvements that increase data collection rates through parallel imaging and faster gradients. At that point, event-related fMRI using rapidly presented stimuli might be the main application to benefit from BOLD signal over IRON signal below 10 T.

When using the IRON method, there are many drawbacks and few advantages of spin-echo sequences, so gradient echoes generally should be employed. The microvascular specificity of spin echoes, as shown in Fig. 17.1, might seem to be a potential advantage. However, the lower overall sensitivity of spin echoes shown in the figure implies that much more contrast agent is required in order to maximize spin-echo CNR. Even then, stimulus-induced increases in CBV will produce smaller signal changes than the gradient-echo method due to the shape of the sensitivity curve versus vessel size; as vessels swell during a functional challenge, sensitivity is reduced (Mandeville et al. 2007b). Furthermore, it is not clear that microvascular sensitivity offers much in the context of IRON fMRI. Whereas the BOLD effect occurs in both capillaries and large veins, the largest relative dilation is observed in microvessels, including small arterioles but not large veins (Hillman et al. 2007). Moreover, the IRON method includes a vascular filter that penalizes large blood volume regions in favor of tissue specificity (Fig. 17.3). The largest gradient-echo IRON signal changes, and the largest relative CBV changes, occur in the middle cortical layers (Mandeville and Marota 1999; Zhao et al. 2006), where capillary density is high, rather than in the superficial cortical surface layers, where the blood volume fraction is highest and the average vessel size is larger (Mandevill et al. 2007b). The practical disadvantages of spin-echo IRON fMRI outweigh any theoretical advantages.

17.4 Arterial Spin Labeling

ASL is a variant of the classical method for measuring blood flow based upon freely diffusible labels. If a label that is carried by the blood is completed extracted into the tissue on the first pass through the capillaries, then the regional concentration of

label will reflect regional blood flow. Ideally, diffusible tracers should satisfy the condition that the product of capillary surface area (S) and the capillary permeability for the tracer (P) is much greater than CBF (PS>>F). For human brain, the PS product for water is marginally larger than flow, and this is less true in smaller animals, which have higher levels of CBF. Because the first-pass extraction of water is incomplete (~80%), water is an imperfect label that underestimates CBF by escaping the tissue through venous flow. PET measurements found that radiolabeled water underestimated CBF by about 15% relative to the use of a more diffusible tracer, butanol (Herscovitch et al. 1987).

In PET experiments, the wash-in of radioactive label is readily measured, as there is essentially no background. For ASL, the effects of blood flow on signal are very weak, and the background represents all brain water except for the small portion of labeled water that flowed into the region. To isolate the flow effect, images are obtained with and without application of RF tagging, and then the images are subtracted. Typically, tagging proximal blood water produces about a 1% effect on MRI signal at clinical field strengths, but this effect is proportional to blood magnetization and so scales with field strength. Obviously, motion between the control and tagged acquisitions will add noise to the flow signal; since the magnitude of motion-induced artifacts scales with the magnitude of signal, this effect can be reduced somewhat by saturating the image volume for all acquisitions (Ye et al. 2000), although this method is not compatible with combined BOLD/ASL measurements.

In terms of measuring blood flow accurately, the main complication for ASL is the short lifetime of the label, rather than the incomplete extraction of water. The MRI method "tags" water magnetically by inverting longitudinal magnetization proximal to the imaging slice, and then observing the distal effects on MRI signal due to blood water that has flowed into the imaging volume. In contrast to the PET method of labeling water using a radioactive oxygen isotope with a decay constant of about 2 min, the MRI label only survives about 1.5 s, which is the T_1 value for arterial water (Lu et al. 2004a). The short duration of the label is both a blessing and curse. On the one hand, rapid elimination of the label allows for repeated experiments on a time scale of seconds in order to follow dynamic changes in CBF or to improve the quality of basal CBF measurements through averaging. On the other hand, the time scale for delivery of blood from the labeling site to the tissue is comparable with the decay time of the label, so that care must be taken to ensure that the measurements really are reporting CBF, as opposed to regional or temporal variations in arrival times between the labeling site and tissue. Transit times can vary either due to variations in the path lengths of vessels or in the flow velocities.

In order to reduce the sensitivity of ASL measurements to transit times, a time delay is inserted after proximal tagging of water in order to ensure that all labeled water arrives in the imaging volume and is properly counted (Alsop and Detre 1996; Wong et al. 1998b). However, this time delay improves accuracy at the cost of sensitivity, because the additional time leads to loss of ASL signal through T_1 decay. Even with a post-labeling delay, transit time's issues produce systematic errors in measurements of CBF under some conditions. The most obvious examples occurs for stroke or vascular disease in humans, where transit times may be greatly extended as a

result of low flow and collateral flow. This cloud may have a silver lining, however, as artifactually low values of flow may improve contrast with normal tissue. A recent study found that ASL detected flow abnormalities in over 40% of patients that had known or suspected vascular disease but normal findings from bolus gadolinium analysis (Zaharchuk et al. 2009).

There are two common variants of ASL that label proximal blood water in fundamentally different ways (Wong et al. 1998a; Williams 2006). Continuous ASL (CASL) tags blood by applying RF radiation to a single slice containing major arteries for extended time periods (1–2 s). This method is conceptually easy to understand, because the amount of labeled water that accumulates in the image volume is proportional to flow and to the time duration of the RF tag, plus a correction factor for decay of the label. Pulsed ASL (PASL) uses a single RF pulse of short duration (milliseconds) to invert water from a proximal slab of tissue. In the absence of any other manipulations of longitudinal magnetization, this method would not measure CBF, because blood is tagged as a volume, rather than as a flow-time product; an upper limit on the ASL signal would occur when all of the tagged blood reached the image volume. To turn PASL into a quantitative method, the spatial tagging scheme is converted to a temporal scheme by saturating the magnetization in the tagging volume after a fixed time delay so that blood remaining in the tagging volume does not contribute to the ASL signal. The selection of PASL tagging widths and timing is crucial for accurate measurements of CBF (Wong et al. 1998b).

Theoretically, CASL provides a large SNR improvement over PASL (Chesler and Kwong 1995; Buxton et al. 1998a), although experimental results in humans have found that actual improvements are less than 50% due to a variety of compensating factors (Wong et al. 1998a; Wang et al. 2002). In animal models on small-bore scanners, the CASL method is almost always employed (e.g., Silva et al. 1995), and this method can be expected to provide larger gains in sensitivity and accuracy relative to PASL as a result of higher CBF and smaller transit times in small animals. Implementation involves separate imaging and labeling RF coils that avoid magnetization transfer effects by physical separation. These small-bore systems always provide a second RF channel for NMR spectroscopy, and this channel can be used to drive the labeling coils using a continuous-wave RF amplifier that is obtained by the user. The CASL implementation is more complicated on human scanners, which don't provide hardware support for a separate RF channel. Instead, implementations use a single RF coil for both labeling and imaging and control off-resonant magnetization transfer using double inversion in the control acquisition (Alsop and Detre 1998). Recent refinements of this method circumvent power limitations and inefficiencies in labeling by using a train of labeling pulses to provide "pseudo-continuous" labeling (Dai et al. 2008).

Given the low detection efficiency for ASL, what is the role of this technique for fMRI? Some authors have argued that the small ASL signal changes may be offset for some applications by less slow-frequency noise in the method (Aguirre et al. 2002) relative to BOLD signal; slow signal drift is particularly problematic for measuring drug-induced responses or other responses that evolve slowly in time. Because ASL is a subtraction method, slow signal drift that is unrelated to physiology will

cancel out in the subtraction. As a general method for brain mapping, however, ASL suffers from smaller signal changes, reduced temporal resolution due to the need to acquire two images for subjections, and few slices per unit time due to the labeling period.

Principally, ASL fills two roles in fMRI by (1) providing data on CBF reactivity to inform simultaneously acquired changes in BOLD signal (e.g., Sect. 17.6.1), and (2) measuring basal CBF in cross sectional BOLD studies to aid interpretation of population differences. The latter function is necessary in principle, at least, because BOLD signal depends upon baseline physiology in addition to functional reactivity. Altered flow states, perhaps as a result of drug exposure or aging or other group differences, can modulate BOLD signal by altering the baseline concentration of deoxygenated hemoglobin (see Eq. 17.1).

17.5 Alternative Methods to Measure CBV

Among alternative methods to measure CBV by MRI, this chapter has focused on the IRON technique due the high CNR of that method. T_1-based measurements using exogenous contrast agent are one obvious alternative method. As discussed previously, such an approach would combine the twin disadvantages of requiring exogenous contrast agent and delivering weak signal changes. While alternative CBV techniques provide signal changes much smaller than the IRON or BOLD methods, nevertheless there has been a desire to develop dynamic methods of measuring CBV without exogenous agent in order to clarify mechanisms of BOLD signal in human subjects.

17.5.1 VASO

Vascular space occupancy (VASO) recently became a popular technique due both to the simplicity of implementation and the potential to assess functional CBV changes in humans (Lu et al. 2003; Lu et al. 2004c). This T_1-based method employs a nonselective preparation pulse to globally invert MRI signal, and tissue and blood then relax back to equilibrium at different rates. Image data are acquired as inverted blood goes through the null point of longitudinal signal recovery. The simplest interpretation for this method posits only two compartments (blood and tissue) that exchange blood water rapidly across the BBB during dilation and contraction of vessels (Lu et al. 2003). In this interpretation, the volume fraction missing from the tissue compartment is CBV. Because VASO is such a weak signal, care must be taken to minimize residual BOLD and flow contributions (Donahue et al. 2006).

The original two-compartment model is incomplete, however, because an increase in CBV requires displacement of other volume. Although bidirectional exchange of water by diffusion across the BBB is a rapid process, unidirectional transport of

water across the BBB under the influence of hydraulic or osmotic pressure is an extremely slow process that is governed by the Starling equation. During focal brain activation, capillary pressure increases as a consequence of arterial dilation, leading to a further increase in the hydraulic pressure gradient across the BBB. However, the direction of this force is opposite to the direction required by the original VASO interpretation, and the magnitude of water exchange is several orders of magnitude too small to be relevant on the time scale of the vascular response (Leite and Mandeville 2007), according to measurements of the hydraulic conductivity of the BBB (Bradbury 1985). Physiological principles suggest that increases in CBV are compensated by decreases in extravascular fluid, with displacement of cerebrospinal fluid (CSF) presumably providing the largest buffer for CBV variation. In fact, a recent study based upon multi-exponential T_2 fitting for CSF and tissue compartments found that CSF reductions were comparable to CBV elevations (Piechnik et al. 2009).

   The extent to which this conceptual objection corrupts the original VASO interpretation is a subject of on-going research. One evaluation of VASO errors found a consistent but insignificant decrease in the CSF fraction in activated regions (Donahue et al. 2006), supporting the authors' original interpretation. A different group reported masking of stimulus-induced activation that might result from dynamic displacement of CSF (Scouten and Constable 2007). However, the most direct evidence that CSF plays a significant role in VASO signal comes from global elevation of CBV by hypercapnia, which produced both positive and negative signal changes using either blood-nulled or CSF-nulled VASO (Scouten and Constable 2008).

   Two strategies have been proposed to reduce the influences of CSF displacement on VASO signal. The first employs a dual inversion preparation to null both blood water and CSF (Donahue et al. 2006). The second strategy combines separate blood-nulling and CSF-nulling steps into a combined index (Scouten and Constable 2008). Relative to the original VASO technique, both methods suffer an SNR penalty but hold promise for making VASO an interpretable signal in terms of isolating a CBV-specific mechanism. However, a final difficulty in relating VASO signal to other indices of functional physiology is that changes in VASO signal are related to changes in CBV without providing any information about basal CBV in any region, so it's not possible to report percent changes in CBV without additional information from another method or by assuming global values for basal CBV; the latter method is unlikely to be accurate except possibly for very large regions of interest that might average away regional differences.

   The original VASO method reported that CBV resolves more slowly to baseline than CBF or BOLD signal (Lu et al. 2003), consistent with results from IRON fMRI. The authors subsequently reported that the slow response of CBV did not co-localize with BOLD and CBF responses, so the BOLD post-stimulus undershoot should be reinterpreted as due to a post-stimulus elevation of $CMRO_2$ (Lu et al. 2004b). In light of the CSF contamination to the VASO signal that since has been demonstrated, it unclear whether VASO signal changes should co-localize with other methods when CSF signal is not controlled. A very recent VASO study that included CSF-nulling found similar responses for CBF and CBV (Donahue et al.

2009). That study used very long single-shot acquisitions in order to increase the temporal efficiency, but this strategy also may dilute the specificity of the VASO signal by bringing in competing mechanisms.

17.5.2   VERVE

VERVE (venous refocusing for volume estimation) is another recently developed method that differs fundamentally from VASO or the use of exogenous contrast agent, in that VERVE aims to measure changes in the venous component of CBV, rather than total CBV. VERVE is derived from BOLD signal, so "venous" is most directly a reference to blood oxygenation in this case, rather to the anatomical definition of veins, which are differentiated from capillaries by smooth muscle.

The VERVE technique (Stefanovic and Pike 2005) takes advantage of the fact that the spin-echo BOLD signal has as substantially larger intravascular than extravascular contribution at clinical field strengths (Zhong et al. 1998; Oja et al. 1999). To further minimize the extravascular contribution, this method uses a subtraction between acquisitions that employ fast and slow refocusing pulses; this subtraction is the VERVE signal. In the absence of T_2 changes in the blood, activation-induced changes in venous CBV could be estimated in a two-compartment blood-tissue model (CSF is nulled) directly from VERVE signal changes. However, venous T_2 does change during activation, so this must be taken into account. This is accomplished by (1) empirical calibration curves for blood T_2 as a function of oxygenation and refocusing interval, and (2) a model for venous oxygenation changes as a function of changes in CBF (Stefanovic and Pike 2005; Chen and Pike 2009a).

There are a number of potential complications in this method that can affect accuracy and limit the general applicability of the method. The method has low sensitivity because it based upon a subtraction of weak BOLD spin-echo signals. Baseline venous blood oxygenation must be assumed or measured. Changes in venous oxygenation are flow-dependent, and estimation of this effect requires a physiological model; simulations demonstrate that this is perhaps a 20% uncertainty. The degree of error induced by extravascular BOLD changes has not yet been quantitatively estimated.

Despite these complications and drawbacks, the method has reported changes in venous blood volume that are not unreasonable, with about a 10% change for a robust stimulus. However, changes in venous CBV reported by the VERVE method don't scale with CBF (Chen and Pike 2009a). There are several potential reasons that VERVE might underestimate venous CBV changes in a way that becomes progressively larger as CBF increases. Potential reasons include an imperfect compensation for intravascular changes in oxygenation, a breakdown in the assumption that extravascular BOLD effects can be ignored even for large changes in CBF, or simply a dynamic range problem that results from the progressive loss of deoxyhemoglobin, the origin of the VERVE signal, at high levels of CBF. Despite low sensitivity

and remaining questions about the quantitative nature of the VERVE signal, this method produced rough agreement with the IRON technique by associating the integrated magnitude of the BOLD post-stimulus undershoot with the integrated magnitude of the CBV response (Chen and Pike 2009b).

17.6   fMRI and Metabolism

17.6.1   *Direct Measurement of CMRO$_2$ Reactivity*

None of the techniques described in this chapter enable insights into glucose metabolism, but BOLD signal is sensitive to oxygen utilization, so information about CMRO$_2$ should be accessible in principle through the BOLD mechanism. For this purpose, a model is required. BOLD signal can be cast into any number of reasonable physical frameworks that are based upon conservation of mass. At the most basic level, BOLD signal is described by oxygen conservation during transit from oxygenated arteries to partially oxygenated veins due to a diffusive loss of blood oxygen into the tissue due for use in metabolism (Ogawa et al. 1993). Viewing the capillaries as a black box, the difference between oxygen flow into and out of the capillaries is the rate of oxygen delivery to the tissue, $F_{IN} - F_{OUT} = dV/dt$, where flow (F) and volume (V) refer to oxygen rather than blood in this equation. This description, discussed below for measurements of CMRO$_2$ reactivity, ignores transit time phenomena such as the time-dependent washout of deoxygenated hemoglobin. It is a steady state model that is not appropriate for describing BOLD changes on a time scale of a few seconds, but this approximation is not bad for BOLD transients of longer duration like the post-stimulus undershoot. For modeling purposes, a better physical framework would apply mass conservation to the blood as well as to the oxygen in order to allow for transient differences between blood flow and volume; this is the Balloon model (Buxton et al. 1998b). If pronounced changes in hematocrit were discovered to occur during functional activation, separate conservation of the plasma and red cell volumes could further extend this model. All physical models of this type conserve mass but say nothing about the underlying physiology.

To determine CMRO$_2$ reactivity, a measurement model must limit the number of free parameters and be relatively insensitive to any parameters that cannot be directly measured. Consider a simple model of BOLD percentage signal changes in terms of fractional changes in CBV (v), CBF (f), and CMRO$_2$ (m):

$$\left.\frac{\Delta S}{S}\right|_{BOLD} = M\left[1 - v\left(\frac{m}{f}\right)^{\beta}\right] \qquad (17.1)$$

The parameter β accounts for a slightly superlinear dependence of the blood relaxation on blood magnetization (Boxerman et al. 1995b). In human studies where

it is difficult to dynamically measure CBV, a coupling relationship is assumed with CBF ($v = f^{\alpha}$) so that

$$\left.\frac{\Delta S}{S}\right|_{\text{BOLD}} = M\left[\, 1 \;-\; m^{\beta}f^{\alpha-\beta}\, \right] \qquad (17.2)$$

The parameter M denotes the maximal possible BOLD signal change. Because BOLD signal reflects the washout of deoxygenated hemoglobin, there is finite headroom for BOLD changes that would be depleted if venous blood became completely oxygenated. M is the product of the echo time and the BOLD-induced relaxation rate (R_2^{BOLD}) during the "resting" or control condition, which in turn depends upon baseline physiology with a proportionality to the local CBV and the ratio of $CMRO_2$ to CBF; the latter is roughly constant across the brain, according to PET measurements (Mazziotta and Phelps 1986). Thus, regional variation in M should roughly reflect regional variations in CBV.

From this description of BOLD signal, it is apparent that the parameter M is playing a role similar to the agent-induced relaxation rate observed upon injection of contrast agent using the IRON method. The latter quantity is readily measurable and is used to normalize signal changes in order to report percentage changes in CBV. For BOLD signal, we can neither estimate changes in $CMRO_2$ nor report percentage changes in deoxyhemoglobin without first finding a way to measure the parameter M. The key insight that enabled BOLD-based measurements of $CMRO_2$ reactivity was that manipulation of blood carbon dioxide levels leads to alterations in blood flow and volume without substantially affecting metabolism, as least on a global basis (Eklöf et al. 1973; Horvath et al. 1994; Yang and Krasney 1995). Therefore, simultaneous BOLD and CBF measurements during hypercapnia can be used to determine M in each image region, and then this value can be used to estimate relative changes in $CMRO_2$ during a metabolically modulated stimulus.

Using this method, experiments in our laboratory were conducted in humans (Davis et al. 1998) and also in rodents (Mandeville et al. 1999a), where IRON fMRI enabled dynamic measurements of CBV as well as CBF. Following the Davis approach, experiments at the Montreal Neurological Institute employed graded hypercapnia and graded visual stimulation to map out an approximately linear coupling in which percentage changes in CBF exceeded percentage changes in $CMRO_2$ (Hoge et al. 1999b). This functional coupling ratio generally has fallen within two to four in healthy human subjects using a variety of stimuli (Davis et al. 1998; Hoge et al. 1999b; Kim et al. 1999; Kastrup et al. 2002; Stefanovic et al. 2004; Uludag et al. 2004; Leontiev et al. 2007).

A number of basic points about the methodology are worth emphasizing. First and foremost, it needs to be emphasized that *details of the model are relatively unimportant if these three assumptions are true*:

Assumption #1): $CMRO_2$ does not change in the region of interest during hypercapnia.

Assumption #2): Hypercapnia and metabolically modulated stimuli produce similar vascular responses in terms of the relationship between CBF and CBV.

The main features of this technique are summarized here:

- While there are several obvious ways to build a more complete theoretical model of BOLD signal, the model presented above enables measurements of $CMRO_2$ reactivity by providing a means to measure M, which depends upon details of the MRI pulse sequence and local physiology. A twofold regional variation in the local blood volume fraction translates into a twofold variation in M, which is such a large range as to render estimations of $CMRO_2$ meaningless when M is not determined empirically on a local basis.
- The method is surprisingly insensitive to uncertainties in α and β due to the "calibration" step provided by the hypercapnia experiment (Davis et al. 1998), particularly when flow changes in the hypercapnic calibration are nearly matched to levels during the metabolically modulated stimulus. When model parameter values are erroneous, the empirical calibration will adjust the model locally to match the data, thereby factoring error into M with little effect on the estimated of $CMRO_2$ reactivity. M reflects the true maximal BOLD signal value (e.g., the resting state BOLD relaxation rate) only to the extent that the model is correct.
- This method fails at very high resolution. The largest BOLD signal changes occur in large draining veins, where ASL signal is small due to the nearly complete extraction of first-pass labeled blood water in the capillaries. For this reason, more accurate estimations of $CMRO_2$ are obtained using large regions of interest or by determining M from pooled subject data as a way of minimizing BOLD/ASL spatial mismatches due to the different vascular weightings of the two techniques (Leontiev et al. 2007).
- Based upon IRON fMRI data obtained in rodents models (Mandeville et al. 1999b) and in non-human primates as reviewed previously, the CBF-CBV coupling relationship (expressed through the parameter α) is not temporally static. CBV continues to increase after CBF and BOLD signal have reached a maximal response. It is important to minimize influences of these transient effects on estimations of $CMRO_2$ reactivity by discounting the first few tens of seconds immediately following onset and cessation of stimulation.

This fMRI technique already has changed some of our previous understandings of flow-metabolism coupling. Of course, PET experiments from the 1980s (Fox and Raichle 1986) discovered that functionally induced changes in $CMRO_2$ were much smaller than changes in CBF and glucose metabolism, an observation that initially was described as "uncoupling" of $CMRO_2$ with CBF and glucose metabolism. Based upon fMRI techniques, it now appears that CBF and $CMRO_2$ couple in very predictable way, but not along the linear trajectory defined by regional CBF-$CMRO_2$ values.

In retrospect, the deviation of $CMRO_2$-CBF coupling from the regional relationship should not have been entirely surprising. As an analogy, regional values of CBF and CBV show a linear coupling; MRI maps of mean transit time, the CBV/CBF ratio, exhibit virtually no contrast in healthy human subjects. However, relative functional changes in CBV are much smaller than corresponding values for CBF (Grubb et al. 1974). Intuitively, these data are reconciled by noting that factors

that govern regional relationships, like angiogenesis during development, are not operable on the time scale of functional activation. In other words, CBF increases as a result of vessel dilation during a functional response, rather than by growing new vessels. This same principle appears to hold true for the CBF-CMRO$_2$ relationship. While capillary density and flow can be adjusted regionally on a long-term basis, the oxygen extraction fraction necessarily falls during a functional response (Buxton and Frank 1997) as a consequence of the relatively constant capillary surface area, which increases only nominally by capillary dilation during functional activation.

This fMRI method of determining CMRO$_2$ reactivity will never generalize to routine functional studies as a result of limited ASL sensitivity. However, the method should prove suitably efficient to investigate targeted questions about neurovascular coupling, such as how to view fMRI results using drugs that alter metabolism but also directly affect vascular smooth muscle. Current questions about methodology concern the accuracy of ASL during global challenges that can dramatically alter blood transit times, and the resolution at which the BOLD model of Eq. 17.1 can be applied to both local and global perturbations without a breakdown due to vascular mixing amongst neighboring voxels.

17.6.2 phMRI in Pharmacology

While there is a burgeoning field of "phMRI" in humans, these studies rarely assess the direct effects of drugs, but rather use traditional fMRI stimulation paradigms with and without drug treatment or pretreatment (Wise and Tracey 2006; Anderson et al. 2008). Assessing the direct effects of drug is more difficult from a detection standpoint, because the response evolves slowly and is not amenable to the repeated on-off paradigms that can control signal drift while building statistical power by within-subject averaging. Human BOLD studies designed to characterize the functional response to drug infusion generally have produced disappointing results. This is not surprising; we obtained poor results using BOLD signal for phMRI at low magnetic fields in animal models (Mandeville et al. 2001; Chen et al. 2001), a result that largely motivated our interest in the IRON technique.

Figure 17.8 illustrates the power of this technique using an example that is relevant for this chapter because it demonstrates an interesting result that can be related to previous gold-standard methods for assessing metabolism, and it also demonstrates the challenges for this method in terms of interpretation. The figure maps the response of CBV to an acute infusion of 0.5 mg/kg cocaine in an awake non-human primate (rhesus). The result is interesting because the sign of the response is opposite the sign of the response in rodents using fMRI (Marota et al. 2000), gold-standard flow methods based upon autoradiography (Stein and Fuller 1993), or measurements of flow and glucose metabolism (Sharkey et al. 1991). However, this species difference between rats and rhesus monkeys previously was reported using the 2-deoxyglucose technique to assess cocaine-induced changes in glucose metabolism (Lyons et al. 1996).
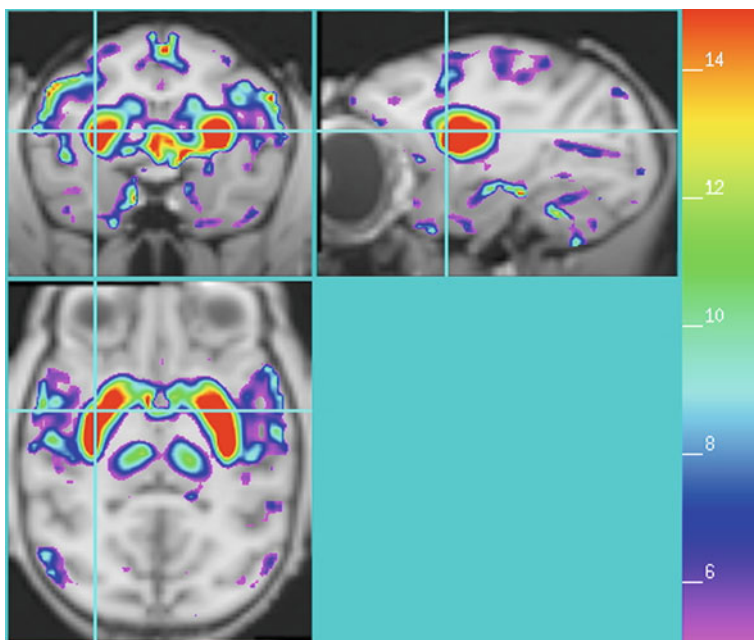
Fig. 17.8 The peak response of CBV in conscious non-human primate following 0.5 mg/kg cocaine infusion is shown using an overlay for negative changes in blood volume. No positive changes in CBV were observed for non-contingent infusion of cocaine, a result opposite to that observed in rodents

This cocaine result also illustrates that fMRI, like metabolism, represents a summation of synaptic consequences that sometimes can be difficult to interpret. Firstly, fMRI measures something very different from PET binding experiments, in that metabolic consequences can be anticipated both at binding sites and in connected circuitry. Even when the drug acts through a single neurotransmitter system like dopamine, post-synaptic receptor binding can be excitatory or inhibitory. Selective D1 and D2 receptor stimulation produce opposite effects on metabolism and fMRI signal (Trugman and James 1993; Marota et al. 2000; Chen et al. 2005), so cocaine might produce opposite effects in the rat and monkey due to different levels of D1 and D2 receptors in these species. Alternatively, cocaine also acts as an indirect serotonergic agonist, producing metabolic modulation through the serotonin system while also potentially reinforce the inhibitory D2 effects. Finally, experiments in conscious animals or human subjects may contain cognitive components in the activation profile.

If fMRI can be viewed as assessing drug-induced metabolism but with the addition of temporal information, what have we gained? One thing we have gained is the ability to employ differential tests in longitudinal studies. The simple assessment of a drug's activation profile represents a differential test relative to the post-drug period, which is not possible with the deoxyglucose approach or with steady-state PET

imaging of receptor binding. Repeated infusions can define the proper timing for drug-antagonist-drug studies, providing within-session differential tests of receptor antagonism, an important statistical advantage relative to across-session comparisons. Selective agonists can be used for comparison of regional activation profiles.

phMRI promises to contribute to our understanding of drug effects in the central nervous system, to evaluate longitudinal changes in response to drug as a consequence of repeated exposure (e.g., addiction) or the evolution of pathology (e.g., Parkinson's disease), and even to characterize cognitive components associated with drug intake in properly designed experiments. The information provided by the method is less interpretable than PET binding studies but also more general, in that assessments of brain function are not limited by available agonists or by the density of receptors in a few target regions. Interpreting the fMRI data will require an accumulation of evidence using multiple agonist or antagonists to dissect sources of signal. Studies of drug-induced brain function using the new generation of combined PET/MR scanners should improve our ability to take advantage of the complementary information provided by these different approaches.

17.6.3   When fMRI Does not Correlate with Metabolism

fMRI does not always correlate with metabolism due to a number of factors that generally are well known but warrant brief discussion. Changing blood levels of carbon dioxide associated with changes in respiration represent a major potential confound. Drug infusion (e.g., opiates) or stressful tasks can alter respiration in free-breathing subjects, leading to non-specific dilation or contraction of cerebral vessels. While CBF, CBV, and BOLD signal are all susceptible to this artifact, BOLD signal has the most sensitivity to CO_2. As discussed in Sect. 17.6.1, metabolically modulated stimuli produce changes in $CMRO_2$, whereas hypercapnia does not. As a consequence, hypercapnia-induced BOLD signal changes are about twice as large as those produced by a visual stimulus for matched changes in blood flow (Hoge et al. 1999a). This means that CO_2-induced BOLD signal changes can be expected to swamp metabolically induced BOLD changes, although changing levels of blood CO_2 are a major problem for other fMRI techniques as well.

Changes in blood pressure appear to be a less significant problem as long as pressure is maintained on autoregulatory plateau between pressures of about 60 and 150 mm Hg. Of course, textbooks properly note that the brain autoregulates CBF between within this range by adjusting arterial diameter, so one might expect fMRI based upon CBV to be susceptible to changes in systemic blood pressure. In fact, our experience has shown IRON fMRI to be surprisingly insensitive to changes in blood pressure. For instance, correlation of signal with large changes in blood pressure due to infusion of an opiate agonist revealed an association in the hypothalamus, a region involved in pressure autoregulation, without significant effects elsewhere in the brain (Liu et al. 2007). This result can be understood by recognizing that the brain regulates perfusion pressure distal to arterioles, so that the dominant

blood volume fraction in the capillaries and veins sees a constant pressure as long as arteries can compensate for the changes in pressure. Progressive reduction of blood pressure in a rodent model showed that BOLD signal and CBV were very insensitive to pressure changes across the autoregulation range (Zaharchuk et al. 1999). BOLD studies in human subjects support this claim (Liu et al. 2006).

17.7 Future Directions

17.7.1 IRON fMRI in Humans?

BOLD signal will continue to be the dominant fMRI contrast mechanism in humans for the foreseeable future, although ASL increasingly is being used to assess baseline physiology in order to aid interpretation of BOLD results. Is it possible that IRON fMRI will become a viable tool for clinical fMRI application? At this time, the only USPIO (ultra-small superparamagnetic) agent approved for use in humans at a dose efficacious for fMRI is Feraheme, which has been approved for the treatment of iron deficiency anemia in adult patients with chronic kidney disease (Coyne 2009). This agent has a blood half-life of 15 h and is approved at a unit dose of 510 mg.

In order to assess the relative detection power using an agent like Feraheme at a dose that has already passed through clinical trials, we validated theoretical CNR calculations as a function of dose (Mandeville et al. 2004) by using sequential doses of Feraheme in an awake non-human primate. Figure 17.9 summarizes the predicted CNR benefits in humans relative to BOLD signal at 1.5 and 3 T. Because the approved dose of iron is not normalized by patient weight, the shaded dose range in the figure includes subjects within the weight range of 50–100 kg. At 1.5 T, the clinical field strength that dominates the market, CNR should be increased roughly fivefold for the average subject. The benefits at 3 T will be smaller, due to larger BOLD signals at that field strength. At ultra-high field strengths like 7 T, currently a field strength limited to research, current dose limitations in human subjects for these types of agents will prevent a benefit relative to BOLD signal.

Fig. 17.9 Predicted boosts in CNR at 1.5 and 3 T using the FDA-approved dose of Feraheme, an iron replacement therapy for patients suffering from chronic iron anemia. The *gray* shaded region approximates the weight-normalized dose for the drug, which was approved for adult subjects without regard to weight
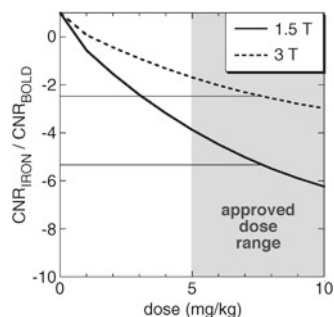
BOLD signal has proven to be an excellent research tool in multi-subject studies for mapping brain regions associated with sensory, motor, and cognitive function in health and disease states. For studies of this type, the ethical and practical burdens to recruiting subjects for IRON fMRI would appear to be unmanageable ("Wanted: OCD subjects who also suffer from iron anemia"), unless iron oxide agents of this type receive wider approval that perhaps is conditional on phlebotomy or assessment of blood iron levels. However, it is not clear IRON fMRI would significantly benefit population studies, where across-subject variance ("random effects" in the fMRI parlance) competes with within-subject variance ("fixed effects").

Individualized medicine may be a different story, in that the limitations of BOLD signal become more pronounced when results must be interpreted on a per-patient basis; limited BOLD sensitivity certainly is among the factors that have inhibited the clinical utility of fMRI within individual patients (Jezzard and Buxton 2006). Preoperative brain mapping prior to tumor resection is one application where the risk-benefit tradeoff might work in favor of IRON fMRI. A single dose of Feraheme represents about 10–15% increase in normal total body iron stores of about 60 mg/kg (Barton et al. 2000). However, further studies will be required to clarify neurovascular coupling in the vicinity of a tumor (Sunaert 2006) and to characterize potential complications due to agent extravasation into tissue near a compromised BBB (Enochs et al. 1999).

Pharmacological stimuli represent a more speculative potential application for IRON fMRI in human subjects. IRON fMRI in animal models have shown excellent within-subject results. For instance, dopamine deficits in a monkey model of Parkinson's disease were probed using a dopaminergic stimulus, and the MRI results correlated with both behavior and PET binding potential (Jenkins et al. 2004). The larger installation base and higher resolution of MRI relative to PET could extend drug stimuli into clinical use as a tool to aid diagnosis or follow treatment.

17.7.2   *Leveraging the Temporal Response of phMRI*

For the vast majority of studies, fMRI provides no differentiation of neural functions based upon temporal response, which is slower than the neuronal response by several orders of magnitude. An exception occurs for pharmacological stimuli, which produce a response that generally evolves so slowly that fMRI directly measures the response of neuronal ensembles. The observation that different regions respond with different kinetics (Marota et al. 2000), and that biphasic responses within an image voxel are observed in some situations (Liu et al. 2007), illustrates that fMRI reflects dynamical responses of the binding targets (receptor or transporter) in addition to drug availability.

Homeostatic feedback mechanisms long have been thought to play some role in governing plastic changes in the brain in response to chronic drug exposure, but emerging evidence suggests that neurotransmitter function may be regulated dynamically even on a timescale of minutes during an acute drug challenge. *In vitro* experiments have identified cellular trafficking of transporters and receptors on this

time scale in response to the rate of stimulation due to the presence of agonist (Johnson et al. 2005; Goodkin et al. 2005; van Rijnsoever et al. 2005). In some cases, fMRI temporal dynamics may offer clues about the origins of signal and the functional connections between brain regions, as we proposed based upon fMRI observations using remifentanil (Liu et al. 2007).

From these fMRI and *in vitro* studies, it is apparent that there is more informa- tion to be gleaned from the temporal response to the drug that simply the average response magnitude, which is generally reported. It will be interesting to see whether specific temporal components of the signal can be blocked by antagonists or modi- fied by drug exposure history. One can imagine that continued improvements in detection power and analysis strategies will significantly increase the information content of phMRI in the near future by exploiting the temporal response.

17.7.3   Physiology Underlying fMRI

fMRI mechanisms can be divided into three main parts: (1) the physics underlying the signal, (2) vascular and metabolic physiology as they contribute to the signal (e.g., CBF-CMRO$_2$ coupling), and (3) the coupling of flow and other fMRI indices to metabolism and neural processing. The last topic is the subject of many chapters in this volume and won't be discussed here. The physics underlying fMRI signal now is pretty well understood. While we know much of the physiology underpin- ning fMRI signals, nevertheless a lot of questions remain.

The main hindrance to a more detailed understanding of BOLD signal relates to measurement limitations *in vivo*. BOLD physiology has proven to be a tough nut to crack mainly due our inability to accurately and dynamically measure CMRO$_2$. PET methods cannot address the temporal response of CMRO$_2$ and have their own limi- tations in terms of accuracy. In MRI or optical studies, CMRO$_2$ is always an invisi- ble variable that can be measured only by inference: essentially, it is the missing oxygen mass not detected by other measurements. This produces an unsatisfying experimental situation that has persisted for almost two decades: CMRO$_2$ can always be invoked to reconcile BOLD data with other measurements (CBF, CBV). Given this situation, it is critical to understand sources of error attached to each of the CBF and CBV methods that are applied in the extraction of CMRO$_2$, and to approach this issue using multiple techniques.

17.7.3.1   What is IRON Signal Measuring?

From a physical viewpoint, we know that changes in IRON signal can be quantita- tively related to changes in the cerebral blood plasma volume (CPV). We typically refer to these changes as "CBV" under the assumption that changes in hematocrit are small enough to be ignored, but this may not be true. Presumably, potential changes in hematocrit would be most pronounced in capillaries, where red blood cells stream in single file, and plasma filling during dilation might occur primarily

in the slow-velocity regions near the vessel walls. However, data on hematocrit during brain activation currently are unavailable, and the complexities of colloidal flow within the multiple blood volume compartments represent a hindrance to accurate modeling of the response. Recent measurements of CBV in humans using VERVE, a method that measures only the CBV contribution to BOLD signal, produces qualitative agreement with the IRON temporal dynamics that have been reported by us and others during the past decade, supporting a role for CBV in the BOLD post-stimulus undershoot (Chen and Pike 2009b).

However, two-photon microscopy, which enables direct visualization of vessel calipers, has produced results that appear to conflict with interpretation of the IRON temporal response as due to a slow venous response. Using this method in a open-skull rat model, venules showed little change in diameter during brain activation, even while optical imaging found a delayed capillary/venous response in a closed-skull model using the same stimulus (Hillman et al. 2007). In terms of relating these results to fMRI, there are two main concerns. The first is that removal of the skull alleviates intracranial pressure, which may alter vascular dynamics in veins, which operate at low pressure. For this reason, it will be important to determine whether opening the skull model, a requirement for very high-resolution optical imaging, affects details of the vascular dynamics like the slow response of IRON signal and the BOLD post-stimulus undershoot. A second concern is whether vessels in the superficial layers of cortex respond similarly with microvessels in deeper layers. The post-stimulus tail of the IRON response has been shown to be much smaller on the cortical surface than in deep cortical tissue (Yacoub et al. 2006).

One reason to better understand IRON signal is to better understand the physiology underlying BOLD signal, which depends upon the volume of deoxygenated hemoglobin, rather than upon CPV or total CBV. If we overestimate the role played by blood volume in BOLD signal, we underestimate the contribution of $CMRO_2$. In terms of BOLD temporal dynamics, it is clear that CBV (or at least CPV) has temporal dynamics that match elements of BOLD dynamics like the post-stimulus undershoot. In fact, IRON temporal dynamics are perhaps the most reproducible correlate to the BOLD undershoot in the literature, so understanding this signal is a good starting point for understanding BOLD dynamics.

To illustrate how uncertainties in the CBV response affect our understanding of BOLD dynamics, let's constrain the space of possible models by the following two postulates: (1) We can ignore changes in hematocrit, so relative changes in CPV, CBV, and red blood cell volume are equivalent, and (2) the relationship between CBF and $CMRO_2$ is governed by limitations on the diffusion rate of oxygen into the extravascular space. The latter assumption follows the Buxton–Frank model (Buxton and Frank 1997) in which fractional changes in $CMRO_2$ (m) are related to fractional changes in flow (f) with a set point that depends upon the baseline oxygen extraction fraction (E_0):

$$m \;=\; \left(1-g_0\right)\frac{f}{E_0}\left[1-\frac{\left(1-E_0\right)^{v/f}}{1-g_0}\right] \tag{17.3}$$

Fig. 17.10 A hypothetic scenario for the BOLD post-stimulus undershoot in which elevation of $CMRO_2$ in the post-stimulus region shifts the BOLD zero-crossing point relative to the CBF-CBV cross-over point
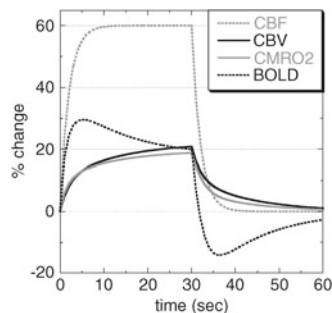
Relative to the original model, this expression includes a tissue oxygen buffer (g_0) that is unchanging for the sake of this discussion (Zheng et al. 2002) and capillary volume expansion expressed as a fractional value (v). A relatively small increase in capillary blood volume (e.g., $v = f^{0.2}$) doubles the $CBF:CMRO_2$ reactivity ratio from 6:1 to 3:1, placing it in much better agreement with published data using the calibrated BOLD method (Sect. 17.6.1). However, even under these relatively restrictive conditions, there are several reasonable hypotheses for the mechanisms underlying the IRON response and the BOLD post-stimulus undershoot that all are consistent with a temporal correlation between BOLD and IRON signals:

Hypothesis #1: *The slow phase of the CBV response is due to stress relaxation in venous smooth muscle, and the BOLD post-stimulus undershoot is attributed to a temporal mismatch between CBF and CBV. Post-stimulus undershoots in CBF may occur for some stimuli as a consequence of neuronal coupling, but this is not a general phenomena, and CMRO$_2$ is temporally linked to CBF. In vitro* experiments in large vessels demonstrate a multi-phase temporal response of diameter in response to a step changes in pressure (Porciuncula et al. 1964), which made this mechanism an attractive solution to the data (Mandeville et al. 1999b). However, stress relaxation seems unlikely to produce such a linear response as shown in the data (Leite et al. 2002; Lu et al. 2005; Silva et al. 2007), and optical microscopy finds minimal changes in venous diameter during the functional response (Hillman et al. 2007).

Hypothesis #2: *The slow phase of the CBV response is due to rate limitations on displacement of CSF within the closed cranium, a mechanism that does not distinguish between capillaries and veins. As a consequence, the BOLD post-stimulus undershoot results from slow decay of both CBV and CMRO$_2$ during the post-stimulus time window after CBF resolves to baseline.* In this scenario, $CMRO_2$ is elevated as a consequence of elevated capillary CBV during the post-stimulus period. Although it seems unlikely that oxygen utilization would be temporally correlated with a mechanical constraint like displacement of CSF, this scenario is presented to highlight the point that the diffusion-limited model does not necessarily imply a temporal coupling of CBF and $CMRO_2$ if capillary CBV follows an altered time course.

This scenario is plotted in Fig. 17.10 for illustrative purposes. Underlying the CBV response is a rapid 50% increase in arterial blood at a 20% blood volume fraction, a slow 20% increase in venous CBV at a 40% blood volume fraction, and a slow 10% increase in capillary CBV at a 40% blood volume fraction. The $CMRO_2$

response was computed from Eq. 17.3, and the BOLD response was computed from Eq. 17.1 and normalized relative to the maximal BOLD response, so that this approximately equals the negative percentage change in deoxygenated hemoglobin.

Hypothesis #3: *The slow phase of the CBV response is due to rate limitations on displacement of CSF. Through a metabolism-flow feedback loop, arteriole diameters adjust flow to temporally regulate CMRO$_2$ to stimulus demands. This requires a post-stimulus undershoot in CBF in response to the post-stimulus elevation of capillary CBV; both effects contribute to the BOLD post-stimulus undershoot, although the mechanical response of CBV is the ultimate cause of the undershoot.* This mechanism temporally couples two phenomena, a slow response of CBV and a post-stimulus undershoot of CBF, which often have been reported in the literature.

The three scenarios above all produce the same multi-phasic CBV response but attribute the BOLD post-stimulus undershoot to either (1) CBV alone, (2) CBV and CMRO$_2$, or (3) CBV and CBF. How might we disentangle these scenarios? In our study in anesthetized rodents (Mandeville et al. 1999a), we observed the post-stimulus undershoot to begin at approximately the "cross-over" point when CBF fell below CBV in the post-stimulus region. Such a simple metric might prove to be more robust than directly calculating CMRO$_2$ through Eq. 17.1, which requires a hypercapnia calibration and which can suffer from error propagated from all the combined measurements. As shown in the simulation of Fig. 17.10, CMRO$_2$ elevation in the post-stimulation region would shift the BOLD undershoot onset relative to the CBF-CBV crossover point.

Not all studies have observed the same temporal dynamics for IRON signal as reported by us (Jin and Kim 2008), and this method is not yet available in human subjects. Evolving techniques like VERVE and VASO may help clarify the physiology underlying the IRON response and its association with BOLD dynamics.

17.7.3.2   Are Changes in CBF and CMRO$_2$ Spatially Variable?

While almost every region of human gray matter has been probed with BOLD signal under some task condition during the past 20 years, a persistent question has been whether or not there are "BOLD silent" regions in the brain or whether some regions intrinsically are harder to map by the BOLD method due to regional variations in the coupling relationship between CMRO$_2$ and CBF. Because BOLD signal in any given brain voxel depends upon the baseline concentration of deoxyhemoglobin, or "M" in the notation of Eq. 17.2, there are expected to be regional differences in the BOLD-CBF coupling ratio and in the BOLD-CBV ratio. From our studies in rats, the measured BOLD-CBV ratio varies by about a factor of 3 across brain, and this variation is completely consistent with the variation in basal CBV, which is easily measured using contrast agent and which should be proportional to "M" (Mandeville et al. 2001). These results suggest that CMRO$_2$-CBF coupling and CMRO$_2$-CBV coupling are regionally invariant.

Hypercapnia calibration in humans has produced a range of results for the coupling ratio of CBF and $CMRO_2$ changes, and much of the variance probably can be ascribed to systematic and statistical measurement errors associated with the methods (Leontiev et al. 2007). A recent study highlights some of the challenges presented by this technique. A combined visual-motor task was used to activate both visual cortex and basal ganglia, and the BOLD to CBF activation ratio was almost threefold smaller in basal ganglia than in visual cortex based upon one criterion for selecting voxels. Unlike our rat study (Mandeville et al. 2001), the hypercapnia calibration technique attributed this variance to the $CMRO_2$-CBF coupling ratio, rather than to "M". While the authors did an extensive review of potential sources of error, the explanation may be rather simple: the method doesn't function well at high resolution. A draining vein from a neighboring voxel may exhibit no oxygenation changes in a voxel of interest for a motor stimulus, but the same vein may dominate BOLD activation in the voxel during a global hypercapnia challenge. Further studies may clarify this issue, but this result demonstrates the challenges of quantifying many aspects of BOLD physiology using available techniques.

17.7.4   Summary

The recent history of fMRI has been one of many incremental improvements that appear small in isolation but ultimately lead to significant improvements in our imaging capabilities. Magnetic field strengths like 7 T that once were labeled as "ultra high" are proliferating. Parallel imaging is only about 10 years old, and already this method is a standard feature on clinical scanners using 32-channel phased array coils or custom-designed arrays with more than 100 elements.

There have been new developments in contrast mechanisms as well. IRON fMRI has become more prevalent in animal studies due to increased availability of contrast agents and continuing demonstrations of efficacy versus other methods, using a wide range of magnetic field strengths and animal models. This method undoubtedly will be extended to human fMRI in the near future, where its long-term role is uncertain. Pseudo-continuous ASL promises to improve the sensitivity and utility of CBF measurements on clinical systems. Persistent efforts to quantify physiologically relevant information using low-SNR endogenous methods like VASO and VERVE are beginning to bear fruit. This broad range of techniques will improve the specificity and accuracy of physiological information provided by fMRI and help clarify remaining uncertainties about the origins of BOLD signal.

References

Aguirre GK, Detre JA, Zarahn E, Alsop DC (2002) Experimental design and the relative sensitivity of BOLD and perfusion fMRI. Neuroimage 15:488–500

Alsop DC, Detre JA (1996) Reduced transit-time sensitivity in noninvasive magnetic resonance imaging of human cerebral blood flow. J Cereb Blood Flow Metab 16:1236–1249

Alsop DC, Detre JA (1998) Multisection cerebral blood flow MR imaging with continuous arterial spin labeling. Radiology 208:410–416

Anderson IM, McKie S, Elliott R, Williams SR, Deakin JF (2008) Assessing human 5-HT function in vivo with pharmacoMRI. Neuropharmacology 55:1029–1037

Axel L (1980) Cerebral blood flow determination by rapid-sequence computed tomography: a theoretical analysis. Radiology 137:679–686

Barton JC, McDonnell SM, Adams PC, Brissot P, Powell LW, Edwards CQ, Cook JD, Kowdley KV (2000) Management of hemochromatosis, vol 1. Cambridge University Press, Cambridge, UK

Belliveau JW, Rosen BR, Betteridge D, Kennedy DN, Vevea JM, Johnson KA, Cohen MS, Weisskoff RM, Rzedzian RR, Brady TJ (1990a) Functional NMR imaging of the human brain. In: Proceedings of the ninth annual meeting of the society of magnetic resonance in medicine, New York, SMRM, p 181

Belliveau JW, Rosen BR, Kantor HL, Rzedzian RR, Kennedy DN, McKinstry RC, Vevea JM, Cohen MS, Pykett IL, Brady TJ (1990b) Functional cerebral imaging by susceptibility-contrast NMR. Magn Reson Med 14:538–546

Belliveau JW, Kennedy DN Jr, McKinstry RC, Buchbinder BR, Weisskoff RM, Cohen MS, Vevea JM, Brady TJ, Rosen BR (1991) Functional mapping of the human visual cortex by magnetic resonance imaging. Science 254:716–719

Boas DA, Jones SR, Devor A, Huppert TJ, Dale AM (2008) A vascular anatomical network model of the spatio-temporal response to brain activation. Neuroimage 40:1116–1129

Boxerman JL, Bandettini PA, Kwong KK, Baker JR, Davis TL, Rosen BR, Weisskoff RM (1995a) The intervascular contributions to fMRI signal change: Monte Carlo modeling and diffusion-weighted studies in vivo. Magn Reson Med 34:4–10

Boxerman JL, Hamberg LM, Rosen BR, Weisskoff RM (1995b) MR contrast due to intravascular magnetic susceptibility perturbations. Magn Reson Med 34:555–566

Boynton GM, Engel SA, Glover GH, Heeger DJ (1996) Linear systems analysis of functional magnetic resonance imaging in human V1. J Neurosci 16:4207–4221

Bradbury MWB (1985) The blood-brain barrier: transport across the cerebral endothelium. Circ Res 57:214–222

Burock MA, Buckner RL, Woldorff MG, Rosen BR, Dale AM (1998) Randomized event-related experimental designs allow for extremely rapid presentation rates using functional MRI. Neuroreport 9:3735–3739

Buxton RB, Frank LR (1997) A model for the coupling between cerebral blood flow and oxygen metabolism during neuronal stimulation. J Cereb Blood Flow Metab 17:64–72

Buxton RB, Frank LR, Wong EC, Siewert B, Warach S, Edelman RR (1998a) A general kinetic model for quantitative perfusion imaging with arterial spin labeling. Magn Reson Med 40:383–396

Buxton RB, Wong EC, Frank LR (1998b) Dynamics of blood flow and oxygenation changes during brain activation: the Balloon model. Magn Reson Med 39:855–864

Buxton RB, Uludag K, Dubowitz DJ, Liu TT (2004) Modeling the hemodynamic response to brain activation. Neuroimage 23(Suppl 1):S220–S233

Chen JJ, Pike GB (2009a) BOLD-specific cerebral blood volume and blood flow changes during neuronal activation in humans. NMR Biomed 22:1054–1062

Chen JJ, Pike GB (2009b) Origins of the BOLD post-stimulus undershoot. Neuroimage 46:559–568

Chen YI, Mandeville JB, Nguyen TV, Talele A, Cavagna F, Jenkins BG (2001) Improved mapping of pharmacologically induced neuronal activation using the IRON technique with Superparamagnetic Iron Blood Pool Agents. J Magn Reson Imaging 14:517–524

Chen YC, Choi JK, Andersen SL, Rosen BR, Jenkins BG (2005) Mapping dopamine D2/D3 receptor function using pharmacological magnetic resonance imaging. Psychopharmacology (Berl) 180(4):705–715

Chesler DA, Kwong KK (1995) An intuitive guide to the T1 based perfusion model. Int J Imaging Syst Tech 6:171–174

Coyne DW (2009) Ferumoxytol for treatment of iron deficiency anemia in patients with chronic kidney disease. Expert Opin Pharmacother 10:2563–2568

Dai W, Garcia D, de Bazelaire C, Alsop DC (2008) Continuous flow-driven inversion for arterial spin labeling using pulsed radio frequency and gradient fields. Magn Reson Med 60:1488–1497

Davis TL, Kwong KK, Weisskoff RM, Rosen BR (1998) Calibrated functional MRI: mapping the dynamics of oxidative metabolism. Proc Natl Acad Sci USA 95:1834–1839

Dennie J, Mandeville JB, Boxerman JL, Packard SD, Rosen BR, Weisskoff RM (1998) NMR imaging of changes in vascular mophology due to tumor angiogenesis. Magn Reson Med 40:793–799

Detre JA, Leigh JS, Williams DS, Koretsky AP (1992) Perfusion Imaging. Magn Reson Med 23:37–45

Dijkhuizen RM, Singhal AB, Mandeville JB, Wu O, Halpern EF, Finklestein SP, Rosen BR, Lo EH (2003) Correlation between brain reorganization, ischemic damage, and neurologic status after transient focal cerebral ischemia in rats: a functional magnetic resonance imaging study. J Neurosci 23:510–517

Donahue KM, Weisskoff RM, Chesler DA, Kwong KK, Bogdanov A Jr, Mandeville JB, Rosen BR (1996) Improving MR quantification of regional blood volume with Intravascular T1 Contrast Agents: accuracy, precision, and water exchange. Magn Reson Med 36:858–867

Donahue MJ, Lu H, Jones CK, Edden RA, Pekar JJ, van Zijl PC (2006) Theoretical and experimental investigation of the VASO contrast mechanism. Magn Reson Med 56:1261–1273

Donahue MJ, Blicher JU, Ostergaard L, Feinberg DA, MacIntosh BJ, Miller KL, Gunther M, Jezzard P (2009) Cerebral blood flow, blood volume, and oxygen metabolism dynamics in human visual and motor cortex as measured by whole-brain multi-modal magnetic resonance imaging. J Cereb Blood Flow Metab 29:1856–1866

Eklöf B, Lassen NA, Nilsson L, Norberg K, Siesjö BK (1973) Blood flow and metabolic rate for oxygen in the cerebral cortex of the rat. Acta Physiol Scand 88:587–589

Engel SA, Glover GH, Wandell BA (1997) Retinotopic organization in human visual cortex and the spatial precision of functional MRI. Cereb Cortex 7:181–192

Enochs WS, Harsh G, Hochberg F, Weissleder R (1999) Improved delineation of human brain tumors on MR images using a long-circulating, superparamagnetic iron oxide agent. J Magn Reson Imaging 9:228–232

Fisel CR, Moore JR, Garrido L, Ackerman JL, Rosen BR, Brady TJ (1989) A general model for susceptibility-based MR contrast. In: Proceedings of the eighth annual meeting of the Society of Magnetic Resonance in Medicine, Amsterdam, p 324

Fox PT, Raichle ME (1986) Focal physiological uncoupling of cerebral blood flow and oxidative metabolism during somatosensory stimulation in human subjects. Proc Natl Acad Sci USA 83:1140–1144

Friston KJ, Mechelli A, Turner R, Price CJ (2000) Nonlinear responses in fMRI: the Balloon model, Volterra kernels, and other hemodynamics. Neuroimage 12:466–477

Goodkin HP, Yeh JL, Kapur J (2005) Status epilepticus increases the intracellular accumulation of GABAA receptors. J Neurosci 25:5511–5520

Grinvald A, Lieke E, Frostig RD, Gilbert CD, Wiesel TN (1986) Functional architecture of cortex revealed by optical imaging of intrinsic signals. Nature 324:361–364

Grubb RL, Raichle ME, Eichling JO, Ter-Pogossian MM (1974) The effects of changes in PaCO2 on cerebral blood volume, blood flow, and vascular mean transit time. Stroke 5:630–639

Hamberg LM, Boccalini P, Stranjalis G, Hunter GJ, Huang Z, Halpern E, Weisskoff RM, Moskowitz MA, Rosen BR (1996) Continuous assessment of relative cerebral blood volume in transient ischemia using steady state susceptibility-contrast MRI. Magn Reson Med 35:168–173

Harel N, Lin J, Moeller S, Ugurbil K, Yacoub E (2006) Combined imaging-histological study of cortical laminar specificity of fMRI signals. Neuroimage 29:879–887

Herscovitch P, Raichle ME, Kilbourn MR, Welch MJ (1987) Positron emission tomographic measurement of cerebral blood flow and permeability-surface area product of water using [15O]water and [11 C]butanol. J Cereb Blood Flow Metab 7:527–542

Hillman EM, Devor A, Bouchard MB, Dunn AK, Krauss GW, Skoch J, Bacskai BJ, Dale AM, Boas DA (2007) Depth-resolved optical imaging and microscopy of vascular compartment dynamics during somatosensory stimulation. Neuroimage 35:89–104

Hoge RD, Atkinson J, Gill B, Crelier GR, Marrett S, Pike GB (1999a) Investigation of BOLD signal dependence on cerebral blood flow and oxygen consumption: the deoxyhemoglobin dilution model. Magn Reson Med 42:849–863

Hoge RD, Atkinson J, Gill B, Crelier GR, Marrett S, Pike GB (1999b) Linear coupling between cerebral blood flow and oxygen consumption in activated human cortex. Proc Natl Acad Sci USA 96:9403–9408

Horvath I, Sandor NT, Ruttner Z, McLaughlin AC (1994) Role of nitric oxide in regulating cerebrocortical oxygen consumption and blood flow during hypercapnia. J Cereb Blood Flow Metab 14:503–509

Jenkins BG, Sanchez-Pernaute R, Brownell AL, Chen YC, Isacson O (2004) Mapping dopamine function in primates using pharmacologic magnetic resonance imaging. J Neurosci 24:9553–9560

Jezzard P, Buxton RB (2006) The clinical potential of functional magnetic resonance imaging. J Magn Reson Imaging 23:787–793

Jin T, Kim SG (2008) Cortical layer-dependent dynamic blood oxygenation, cerebral blood flow and cerebral blood volume responses during visual stimulation. Neuroimage 43:1–9

Johnson LA, Furman CA, Zhang M, Guptaroy B, Gnegy ME (2005) Rapid delivery of the dopamine transporter to the plasmalemmal membrane upon amphetamine stimulation. Neuropharmacology 49:750–758

Kastrup A, Kruger G, Neumann-Haefelin T, Glover GH, Moseley ME (2002) Changes of cerebral blood flow, oxygenation, and oxidative metabolism during graded motor activation. Neuroimage 15:74–82

Kennan RP, Scanley BE, Gore JC (1997) Physiologic basis for BOLD MR signal changes due to hypoxia/hyperoxia: separation of blood volume and magnetic susceptibility effects. Magn Reson Med 37:953–956

Kennan RP, Scanley BE, Innis RB, Gore JC (1998) Physiological basis for BOLD MR signal changes due to neuronal stimulation: separation of blood volume and magnetic susceptibility effects. Magn Reson Med 40:840–846

Kety S (1960) Measurement of local blood flow by the exchange on an inert diffusible substance. Methods Med Res 8:228–236

Kida I, Rothman DL, Hyder F (2007) Dynamics of changes in blood flow, volume, and oxygenation: implications for dynamic functional magnetic resonance imaging calibration. J Cereb Blood Flow Metab 27:690–696

Kim SG, Rostrup E, Larsson HB, Ogawa S, Paulson OB (1999) Determination of relative CMRO2 from CBF and BOLD changes: significant increase of oxygen consumption rate during visual stimulation. Magn Reson Med 41:1152–1161

Kong Y, Zheng Y, Johnston D, Martindale J, Jones M, Billings S, Mayhew J (2004) A model of the dynamic relationship between blood flow and volume changes during brain activation. J Cereb Blood Flow Metab 24:1382–1392

Kruger G, Glover GH (2001) Physiological noise in oxygenation-sensitive magnetic resonance imaging. Magn Reson Med 46:631–637

Kruger G, Kastrup A, Glover GH (2001) Neuroimaging at 1.5 T and 3.0 T: comparison of oxygenation-sensitive magnetic resonance imaging. Magn Reson Med 45:595–604

Kwong K, Belliveau J, Chesler D, Goldberg I, Weisskoff R, Poncelet B, Kennedy D, Hoppel B, Cohen M, Turner R, Cheng H, Brady T, Rosen B (1992) Dynamic magnetic resonance imaging of human brain activity during primary sensory stimulation. Proc Natl Acad Sci 89:5675–5679

Lee SP, Silva AC, Ugurbil K, Kim SG (1999) Diffusion-weighted spin-echo fMRI at 9.4 T: microvascular/tissue contribution to BOLD signal changes. Magn Reson Med 42:919–928

Leite FP (2006) Detection power, temporal response, and spatial resolution of IRON fMRI in awake, behaving monkeys at 3 Tesla. Massachusetts Institute of Technology, Cambridge, MA

Leite FP, Mandeville JB (2006) Characterization of event-related designs using BOLD and IRON fMRI. Neuroimage 29:901–909

Leite FP, Mandeville JB (2007) Investigating water exchange across the BBB as a mechanism for the slow time constant of blood volume. In: Proceedings of the International Society for Magnetic Resonance in Medicine, Berlin, p 3190

Leite FP, Tsao D, Vanduffel W, Fize D, Sasaki Y, Wald LL, Dale AM, Kwong KK, Orban GA, Rosen BR, Tootell RB, Mandeville JB (2002) Repeated fMRI using Iron Oxide Contrast Agent in Awake, behaving macaques at 3 Tesla. Neuroimage 16:283–294

Leite FP, Vanduffel W, Rosen BR, Mandeville JB (2005) Comparing spatial resolution of IRON and BOLD in awake macaques. In: Proceedings of the International Society for Magnetic Resonance in Medicine, Miami Beach, p 303

Leontiev O, Dubowitz DJ, Buxton RB (2007) CBF/CMRO2 coupling measured with calibrated BOLD fMRI: sources of bias. Neuroimage 36:1110–1122

Liu H, Rainey C, Lauer KK, Piacentine L, Bloom A, Risinger R, Ward BD, Stein E, Li SJ (2006) Peripheral blood pressure changes induced by dobutamine do not alter BOLD signals in the human brain. Neuroimage 30:745–752

Liu CH, Greve DN, Dai G, Marota JJ, Mandeville JB (2007) Remifentanil administration reveals biphasic phMRI temporal responses in rat consistent with dynamic receptor regulation. Neuroimage 34:1042–1053

Lu H, Golay X, Pekar JJ, Van Zijl PC (2003) Functional magnetic resonance imaging based on changes in vascular space occupancy. Magn Reson Med 50:263–274

Lu H, Clingman C, Golay X, van Zijl PC (2004a) Determining the longitudinal relaxation time (T1) of blood at 3.0 Tesla. Magn Reson Med 52:679–682

Lu H, Golay X, Pekar JJ, Van Zijl PC (2004b) Sustained poststimulus elevation in cerebral oxygen utilization after vascular recovery. J Cereb Blood Flow Metab 24:764–770

Lu H, van Zijl PC, Hendrikse J, Golay X (2004c) Multiple acquisitions with global inversion cycling (MAGIC): a multislice technique for vascular-space-occupancy dependent fMRI. Magn Reson Med 51:9–15

Lu H, Soltysik DA, Ward BD, Hyde JS (2005) Temporal evolution of the CBV-fMRI signal to rat whisker stimulation of variable duration and intensity: a linearity analysis. Neuroimage 26: 432–440

Lyons D, Friedman DP, Nader MA, Porrino LJ (1996) Cocaine alters cerebral metabolism within the ventral striatum and limbic cortex of monkeys. J Neurosci 16:1230–1238

Mandeville JB, Marota JJA (1999) Vascular filters of functional MRI: spatial localization using BOLD and CBV contrast. Magn Reson Med 42:591–598

Mandeville JB, Marota JJA, Kosofsky BE, Keltner JR, Weissleder R, Rosen BR, Weisskoff RM (1998) Dynamic functional imaging of relative cerebral blood volume during rat forepaw stimulation. Magn Reson Med 39:615–624

Mandeville JB, Marota JJA, Ayata C, Moskowitz MA, Weisskoff RM, Rosen BR (1999a) An MRI measurement of the temporal evolution of relative CMRO2 during rat forepaw stimulation. Magn Reson Med 42:944–951

Mandeville JB, Marota JJA, Ayata C, Zaharchuk G, Moskowitz MA, Rosen BR, Weisskoff RM (1999b) Evidence of a cerebrovascular post-arteriole windkessel with delayed compliance. J Cereb Blood Flow Metab 19:679–689

Mandeville JB, Jenkins BG, Kosofsky BE, Moskowitz MA, Rosen BR, Marota JJA (2001) Regional Sensitivity and Coupling of BOLD and CBV Changes during Stimulation of Rat Brain. Magn Reson Med 45:443–447

Mandeville JB, Jenkins BG, Chen YC, Choi JK, Kim YR, Belen D, Liu C, Kosofsky BE, Marota JJ (2004) Exogenous contrast agent improves sensitivity of gradient-echo functional magnetic resonance imaging at 9.4 T. Magn Reson Med 52:1272–1281

Mandeville JB, Leite FP, Marota JJ (2007a) Spin-echo MRI underestimates functional changes in microvascular cerebral blood plasma volume using exogenous contrast agent. Magn Reson Med 58:769–776

Mandeville JB, Liu C, Marota JJA (2007) Spin echoes underestimate functional changes in micro-vascular cerebral blood volume. In: Proceedings of the International Society for Magnetic Resonance in Medicine, Berlin, p 770

Marota JJA, Ayata C, Moskowitz MA, Weisskoff RM, Rosen BR, Mandeville JB (1999) Investigation of the early response to rat forepaw stimulation. Magn Reson Med 41:247–252

Marota JJA, Mandeville JB, Weisskoff RM, Moskowitz MA, Rosen BR, Kosofsky BE (2000) Cocaine activation discriminates dopamergic projections by temporal response: an fMRI study in rat. Neuroimage 11:13–23

Mazziotta JC, Phelps ME (1986) Positron emission tomography studies of the brain. Raven Press, New York

Meier P, Zierler KL (1954) On the theory of the indicator-dilution method for measurement of blood flow and volume. J Appl Physiol 6:731–744

Ogawa S, Lee TM (1990) Magnetic resonance imaging of blood vessels at high fields: in vivo and in vitro measurements and image simulation. Magn Reson Med 16:9–18

Ogawa S, Lee TM, Kay AR, Tank DW (1990a) Brain magnetic resonance imaging with contrast dependent on blood oxygenation. Proc Natl Acad Sci USA 87:9868–9872

Ogawa S, Lee TM, Nayak AS, Glynn P (1990b) Oxygenation-sensitive contrast in magnetic reso-nance image of rodent brain at high magnetic fields. Magn Reson Med 14:68–78

Ogawa S, Lee RM, Barrere B (1993) The sensitivity of magnetic resonance image signals of a rat brain to changes in the cerebral venous blood oxygenation. Magn Reson Med 29:205–210

Oja JM, Gillen J, Kauppinen RA, Kraut M, van Zijl PC (1999) Venous blood effects in spin-echo fMRI of human brain. Magn Reson Med 42:617–626

Parkes LM, Schwarzbach JV, Bouts AA, Deckers RH, Pullens P, Kerskens CM, Norris DG (2005) Quantifying the spatial resolution of the gradient echo and spin echo BOLD response at 3 Tesla. Magn Reson Med 54:1465–1472

Pauling L, Coryell CD (1936) The magnetic properties and structure of hemoglobin. Oxyhemoglobin and carbon monooxyhemoglobin. Proc Natl Acad Sci USA 22:210–216

Piechnik SK, Evans J, Bary LH, Wise RG, Jezzard P (2009) Functional changes in CSF volume estimated using measurement of water T2 relaxation. Magn Reson Med 61:579–586

Porciuncula CI, Armstrong JGG, Guyton AC, Stone HL (1964) Delayed compliance in external jugular vein of the dog. Am J Physiol 207:728–732

Rosen BR, Belliveau JW, Vevea JM, Brady TJ (1990) Perfusion Imaging with NMR contrast agents. Magn Reson Med 14:249–265

Rosen BR, Belliveau JW, Aronen HJ, Kennedy D, Buchbinder BR, Fischman A, Gruber M, Glas J, Weisskoff RM, Cohen MS, Hochberg FH, Brady TJ (1991) Susceptibility contrast imaging of cerebral blood volume: human experience. Magn Reson Med 22:293–299

Roy CS, Sherrington CS (1890) On the regulation of the blood-supply of the brain. J Physiol (London) 11:85–108

Royl G, Leithner C, Kohl M, Lindauer U, Dirnagl U, Kwong K, Mandeville JB (2001) The BOLD post-stimulus undershoot: fMRI versus imaging spectroscopy. In: Proceedings of the International Society for Magnetic Resonance in Medicine, Glasgow, p 282

Scouten A, Constable RT (2007) Applications and limitations of whole-brain MAGIC VASO func-tional imaging. Magn Reson Med 58:306–315

Scouten A, Constable RT (2008) VASO-based calculations of CBV change: accounting for the dynamic CSF volume. Magn Reson Med 59:308–315

Sharkey J, McBean DE, Kelly PAT (1991) Acute cocaine administration: effects on local cerebral blood flow and metabolic demand in the rat. Brain Res 548:310–314

Shen T, Weissleder R, Papisov MA, Bogdanov J, Brady TJ (1993) Monocrystalline iron oxide nanocompounds (MION): physiochemical properties. Magn Reson Med 29:599–604

Shmuel A, Yacoub E, Chaimow D, Logothetis NK, Ugurbil K (2007) Spatio-temporal point-spread function of fMRI signal in human gray matter at 7 Tesla. Neuroimage 35:539–552

Silva AC, Zhang W, Williams DS, Koretsky AP (1995) Multi-slice MRI of rat brain perfusion dur-ing amphetamine stimulation using arterial spin labeling. Magn Reson Med 33:209–214

Silva AC, Koretsky AP, Duyn JH (2007) Functional MRI impulse response for BOLD and CBV contrast in rat somatosensory cortex. Magn Reson Med 57:1110–1118

Song AW, Wong EC, Tan SG, Hyde JS (1996) Diffusion weighted fMRI at 1.5 T. Magn Reson Med 35:155–158

Stefanovic B, Pike GB (2005) Venous refocusing for volume estimation: VERVE functional magnetic resonance imaging. Magn Reson Med 53:339–347

Stefanovic B, Warnking JM, Pike GB (2004) Hemodynamic and metabolic responses to neuronal inhibition. Neuroimage 22:771–778

Stein EA, Fuller SA (1993) Cocaine's time action profile on regional cerebral blood flow in the rat. Brain Res 626:117–126

Sunaert S (2006) Presurgical planning for tumor resectioning. J Magn Reson Imaging 23:887–905

Ter-Pogossian MM, Eichling JO, Davis DO, Welch MJ, Metzger JM (1969) The determination of regional cerebral blood flow by means of water labeled with radioactive oxygen 15. Radiology 93:31–40

Thulborn KR, Waterton JC, Radda GK (1981) Proton Imaging for in vivo blood flow and oxygen consumption measurements. Journal of Magn Reson 45:188–191

Thulborn KR, Waterton JC, Matthews PM, Radda GK (1982) Oxygenation dependence of the transverse relaxation time of water protons in whole blood at high field. Biochim Biophys Acta 714:265–270

Tootell RBH, Switkes E, Silverman MS, Hamilton SL (1988) Functional anatomy of macaque striate cortex. II. Retinotopic Organization. J Neurosci 8:1531–1568

Triantafyllou C, Hoge RD, Krueger G, Wiggins CJ, Potthast A, Wiggins GC, Wald LL (2005) Comparison of physiological noise at 1.5 T, 3 T and 7 T and optimization of fMRI acquisition parameters. Neuroimage 26:243–250

Tropres I, Gramault S, Vaeth A, Grillon E, Julien C, Payen J-F, Lamalle L, Decorps M (2001) Vessel size imaging. Magn Reson Med 45:397–408

Trugman JM, James CL (1993) D1 dopamine agonist and antagonist effects on regional cerebral glucose utilization in rats with intact dopaminergic innervation. Brain Res 607:270–274

Tsao DY, Vanduffel W, Sasaki Y, Fize D, Knutsen TA, Mandeville JB, Wald LL, Dale AM, Rosen BR, Van Essen DC, Livingstone MS, Orban GA, Tootell RB (2003) Stereopsis activates V3A and caudal intraparietal areas in macaques and humans. Neuron 39:555–568

Tsao DY, Freiwald WA, Tootell RB, Livingstone MS (2006) A cortical region consisting entirely of face-selective cells. Science 311:670–674

Uludag K, Dubowitz DJ, Yoder EJ, Restom K, Liu TT, Buxton RB (2004) Coupling of cerebral blood flow and oxygen consumption during physiological activation and deactivation measured with fMRI. Neuroimage 23:148–155

van Bruggen N, Busch E, Palmer JT, Williams SP, de Crespigny AJ (1998) High-resolution functional magnetic resonance imaging of the rat brain: mapping changes in cerebral blood volume using iron oxide contrast media. J Cereb Blood Flow Metab 18:1178–1183

van Rijnsoever C, Sidler C, Fritschy JM (2005) Internalized GABA-receptor subunits are transferred to an intracellular pool associated with the postsynaptic density. Eur J Neurosci 21:327–338

Vanduffel W, Fize D, Mandeville JB, Nelissen K, Van Hecke P, Rosen BR, Tootell RBH, Orban GA (2001) Visual motion processing investigated using contrast-enhanced fMRI in awake behaving monkeys. Neuron 32:565–577

Villringer A, Rosen BR, Belliveau JW, Ackerman JL, Lauffer RB, Buxton RB, Chao Y, Wedeen VJ, Brady TJ (1988) Dynamic imaging with lanthanide chelates in normal brain: contrast due to magnetic susceptibility effects. Magn Reson Med 6:164–174

Wang J, Alsop DC, Li L, Listerud J, Gonzalez-At JB, Schnall MD, Detre JA (2002) Comparison of quantitative perfusion imaging using arterial spin labeling at 1.5 and 4.0 Tesla. Magn Reson Med 48:242–254

Weissleder R, Elizondo G, Wittenberg K (1990) Ultrasmall superparamagnetic iron oxide. Characterization of a new class of contrast agents for MR imaging. Radiology 175:489–493

Williams DS (2006) Quantitative perfusion imaging using arterial spin labeling. Methods Mol Med 124:151–173

Williams DS, Detre JA, Leigh JS, Koretsky AP (1992) Magnetic resonance imaging of perfusion using spin inversion of arterial water. Proc Natl Acad Sci USA 89:212–216

Wise RG, Tracey I (2006) The role of fMRI in drug discovery. J Magn Reson Imaging 23: 862–876

Wong EC, Buxton RB, Frank LR (1998a) A theoretical and experimental comparison of continuous and pulsed arterial spin labeling techniques for quantitative perfusion imaging. Magn Reson Med 40:348–355

Wong EC, Buxton RB, Frank LR (1998b) Quantitative imaging of perfusion using a single subtraction (QUIPSS and QUIPSS II). Magn Reson Med 39:702–708

Yacoub E, Ugurbil K, Harel N (2006) The spatial dependence of the poststimulus undershoot as revealed by high-resolution BOLD- and CBV-weighted fMRI. J Cereb Blood Flow Metab 26:634–644

Yang SP, Krasney JA (1995) Cerebral blood flow and metabolic responses to sustained hypercapnia in awake sheep. J Cereb Blood Flow Metab 15:115–123

Ye FQ, Frank JA, Weinberger DR, McLaughlin AC (2000) Noise reduction in 3D perfusion imaging by attenuating the static signal in arterial spin tagging (ASSIST). Magn Reson Med 44:92–100

Zaharchuk G (2007) Theoretical basis of hemodynamic MR imaging techniques to measure cerebral blood volume, cerebral blood flow, and permeability. AJNR Am J Neuroradiol 28:1850–1858

Zaharchuk G, Mandeville JB, Bogdonov AA Jr, Weissleder R, Rosen BR, Marota JJA (1999) Cerebrovascular dynamics of autoregulation and hypotension: an MRI study of CBF and changes in total and microvascular cerebral blood volume during hemorrhagic hypotension. Stroke 30:2197–2205

Zaharchuk G, Bammer R, Straka M, Shankaranarayan A, Alsop DC, Fischbein NJ, Atlas SW, Moseley ME (2009) Arterial spin-label imaging in patients with normal bolus perfusion-weighted MR imaging findings: pilot identification of the borderzone sign. Radiology 252:797–807

Zhao F, Wang P, Hendrich K, Ugurbil K, Kim SG (2006) Cortical layer-dependent BOLD and CBV responses measured by spin-echo and gradient-echo fMRI: insights into hemodynamic regulation. Neuroimage 30:1149–1160

Zheng Y, Martindale J, Johnston D, Jones M, Berwick J, Mayhew J (2002) A model of the hemodynamic response and oxygen delivery to brain. Neuroimage 16:617–637

Zhong J, Kennan RP, Fulbright RK, Gore JC (1998) Quantification of intravascular and extravascular contributions to BOLD effects induced by alteration in oxygenation or intravascular contrast agents. Magn Reson Med 40:526–536